PURPOSE-LED PUBLISHING™

TUTORIAL • **OPEN ACCESS**

Geometric phases and holonomy in structured optical fields—a tutorial

To cite this article: Kristina Frizyuk *et al* 2026 *J. Opt.* **28** 113501

View the article online for updates and enhancements.

You may also like

- A common-path caustic interferometer for independent control of petal number, contrast, and orientation
Yaxun Zhang, Xun Hou and Dongmei Deng
- Ultrafast pulse dynamics in a transport-compatible phase-space representation
Anvarjon Sherniyozov, Azamat Japaqov, Feruza Shermatova et al.
- Perturbative analysis of the Wood anomalies of metallic diffraction gratings
Juan David Castrillón-Gómez and Eugenio R Méndez

4-CHANNEL CONFIGURABLE OPEN RF ENGINE FOR QUANTUM EXPERIMENTS

LUGUS

Developed by Instrumentation Technologies

High bandwith arbitraty waveform generator (AWG)
Up to 1.25 GSPS

Open & programmable
Full access to FPGA implementation and firmware

Compatible with control frameworks
LabScript, ARTIQ, etc.

High power outputs
Up to 36 dBm

High-bandwidth feedback control
Open or closed-loop operation, Feedback bandwidth up to 125 MSPS

This content was downloaded from IP address 129.13.194.163 on 09/11/2026 at 06:56

Journal of Optics

Check for updates

TUTORIAL

OPEN ACCESS

RECEIVED
15 June 2026

REVISED
27 September 2026

ACCEPTED FOR PUBLICATION
19 October 2026

PUBLISHED
2 November 2026

Original content from this work may be used under the terms of the Creative Commons Attribution 4.0 licence.

Any further distribution of this work must maintain attribution to the author(s) and the title of the work, journal citation and DOI.

Geometric phases and holonomy in structured optical fields—a tutorial

Kristina Frizyuk[1,*], **Evgenii Menshikov**[2] and **Mauro Spera**[3]

[1] Institute of Theoretical Solid State Physics, Karlsruhe Institute of Technology, Karlsruhe, Germany
[2] Department of Information Engineering, University of Brescia, Brescia, Italy
[3] Dipartimento di Matematica e Fisica 'Niccolò Tartaglia, Università Cattolica del Sacro Cuore, Brescia, Italy
[*] Author to whom any correspondence should be addressed.

E-mail: kristina.friziuk@kit.edu

Keywords: geometric phase, structured light, vortex beams, total angular momentum, nanostructures

Abstract

Geometric phases are widely used in modern optics, yet their meaning and underlying geometry depend on the actual physical settings, which can substantially differ from one another. This tutorial article introduces geometric phases in nanophotonic systems, focusing on the interaction of structured light with nanostructures or metaatoms. We compare the present setting with conventional geometric phases of structured-light optics and show that similar phase laws may correspond to genuinely different underlying geometries. Our aim is to provide a pedagogical bridge between the mathematical language of geometric phases and experimentally relevant examples from nanophotonics.

1. Introduction

Geometric phases are widely used in optics [1, 2] for different applications. The simplest one is transmission of a polarized plane wave through a waveplate [3, 4], corresponding to the rotation of the Poincaré sphere around a horizontal axis. Among the best-known examples we find the Pancharatnam–Berry metasurfaces, which use the orientation of anisotropic metaatoms to control the phase of the cross-polarized component [5–7]. This principle has enabled dielectric metalenses [8] and reflective metasurface holograms [9, 10]. Patterned liquid-crystal elements provide a related implementation [11], while metaatoms with higher-fold rotational symmetries can realize generalized Pancharatnam–Berry phases [12, 13].

Geometric phases can also be introduced for beams with angular momentum through the associated Poincaré-sphere representation [14–16]. Their extension to higher-order transverse modes is discussed, for example, in [17, 18], see also the review [1]. Geometric phases arise in distinct optical settings and need not share the same underlying geometry. Besides the conventional Pancharatnam–Berry phase of polarization evolution, they occur in polarization transport along curved optical trajectories [19, 20], in polarization-dependent beam shifts and reflected structured fields [21, 22], and in geometrically twisted optical resonators [23]. Distinct geometrical structures also arise for fixed-helicity states in momentum space [24] and for higher-order spatial modes on Hermite–Laguerre modal spheres [25].

The following question then arises: why are these particular types of phases called 'geometric'? What is then the underlying geometry? This question has been initially addressed in [26], which connects the phase, introduced by Berry with the holonomy of a connection on a line bundle. Here, we discuss the geometric phases for vortex beams from this point of view, via an explicit description of the underlying topological and geometrical objects, comparing two different types of possible phases. The effect enables mode-selective phase control and discrimination of vortex beams based on their total angular momentum (TAM), using simple nanostructures, offering a practical alternative to spatial light modulators and multi-element polarization schemes.

© 2026 The Author(s). Published by IOP Publishing Ltd

We first start with the description of the simplest well-known case of a waveplate and circularly polarized plane waves, and later generalize it by introducing an analogous geometric phase for optical beams. Then we provide a mathematical description of the well-known geometric phase for beams, showing the emergence of a different geometry.

The paper is organized as follows: in section 2 we revisit the well-known Pancharatnam geometric phase and describe its geometry in detail. In section 3 we describe a direct Pancharatnam–Berry-phase analogy for vortex beams. In section 4 we discuss the usual geometric phase of higher-order transverse modes and show that its underlying geometry is different. In section 5, we compare different Poincaré sphere constructions. In section 6, we compare these geometrical descriptions and discuss open conceptual issues concerning geometric phases in linear and nonlinear optics.

The guiding point of this work is the observation that in order to assign a geometric or topological meaning to an optical phase, one must first specify the bundle structure over the relevant base space [24, 27]. Only then can notions such as connection, holonomy, curvature, or topological invariants be accommodated and acquire a precise meaning. Accordingly, we focus not only on the accumulated phase, but also on the underlying geometry.

This tutorial is intended both for readers working in structured light, nanophotonics, and optical angular momentum, and for mathematically oriented readers interested in concrete physical examples of geometric phases. Polarization optics offers perhaps one of the simplest experimentally accessible, yet mathematically nontrivial, settings in which the notions of state space, base space, connection, and holonomy can be observed explicitly. We use this example as a starting point for comparing related optical phase effects and clarifying the geometrical structures behind them.

Recent reviews cover the historical development and experimental realizations of geometric phases [28], as well as wavefront control and waveguiding [29]. Their implementation in metasurfaces has been reviewed in [30], while nonlinear geometric phases have been considered separately in [31]. For structured optical fields, we also use TAM projections, which more directly reflect the rotational symmetry of the full electromagnetic field.

A comment on terminology is mandatory at this point. Pancharatnam introduced the geometric phase in polarization optics through the interference of differently polarized states [3], whereas Berry introduced geometric phase for the description of cyclic adiabatic evolution of quantum states [32]. Later on he established the precise relation between the two constructions [4]. In the two-state polarization problem considered here, they share the same underlying geometrical structure. The term Pancharatnam–Berry phase is commonly used in optics for this polarization geometric phase and does not relate to a third distinct effect. Accordingly, in this context, we do not distinguish between the terms Pancharatnam phase and Pancharatnam–Berry phase, and use the term Berry phase when referring to the same construction from the more general geometrical viewpoint.

2. The simplest case of the Pancharatnam phase

In this section, we describe the case of a polarized wave passing through a waveplate in some detail [33–35].

2.1. Poincaré and Riemann sphere

The polarization state of light $\mathbf{E}$ in the basis of right $|R\rangle$ and left-circularly polarized $|L\rangle$ plane waves (RCP and LCP, respectively) can be described by two complex numbers $(E_R, E_L) \in \mathbb{C}^2$:

$$\mathbf{E} = E_R|R\rangle + E_L|L\rangle = E_x|B_e\rangle + E_y|B_o\rangle \tag{1}$$

where

$$|B_e\rangle = \frac{|R\rangle + |L\rangle}{\sqrt{2}}, \qquad |B_o\rangle = -\mathrm{i}\,\frac{|R\rangle - |L\rangle}{\sqrt{2}}, \tag{2}$$

and E_R and E_L are complex numbers that fully encode the field state. After normalization,

$$\hat{\Psi} = \frac{1}{\sqrt{|E_R|^2 + |E_L|^2}} \begin{pmatrix} E_R \\ E_L \end{pmatrix}, \tag{3}$$

the pair of complex amplitudes satisfies $|E_R|^2 + |E_L|^2 = 1$ and therefore lies on the three-sphere $S^3 \subset \mathbb{C}^2 \simeq \mathbb{R}^4$. However, for determining polarization states, only the relative amplitude and phase matter;

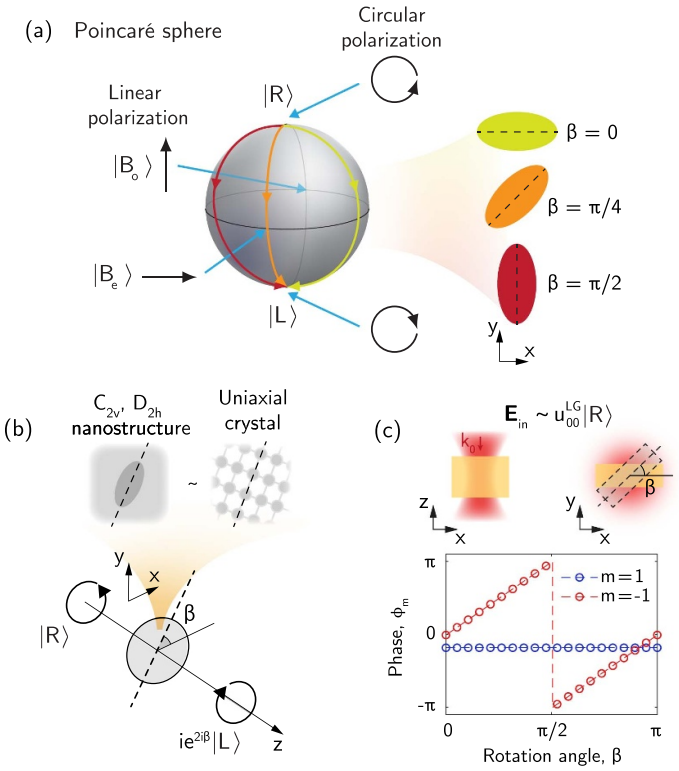


Figure 1. Poincaré sphere and examples of nanostructures for a geometric-phase experiment. (a) Depending on the rotation β of the structure, the Poincaré sphere rotates around different axes. The path corresponds to the case where incident RCP light is converted to LCP light upon transmission through such a structure. (b) Schematic of the setup illustrating geometric phase. (c) Numerically calculated phase acquired upon rotation of a cuboid nanoparticle under excitation by a fundamental Gaussian beam. The phase is wrapped to the range $[-\pi, \pi]$, circular markers indicate the calculated points, the dashed lines are guides to the eye.

not only the overall amplitude but also global phase factor are irrelevant. Let us introduce the vector:

$$\mathbf{\Psi} = \begin{pmatrix} E_R \\ E_L \end{pmatrix}, \tag{4}$$

which is analogous to the Jones vector for linear polarization. Since the overall amplitude and phase of $\mathbf{\Psi}$ do not affect the polarization state, we can normalize this vector and consider only the ratio of E_R to E_L, represented as a complex number $z = E_R/E_L$. The complex plane may be compactified to a Riemann sphere, with homogeneous coordinates $[E_R : E_L]$ (see appendix B). The Poincaré sphere then provides a way of parametrizing polarization states in a unique fashion. The mapping from the complex plane to the Poincaré sphere is given by the stereographic projection (see appendix A and [36]):

$$z = \cot\left(\frac{\theta}{2}\right) \mathrm{e}^{-\mathrm{i}\varphi}, \tag{5}$$

where θ is the polar angle from the north pole of the Poincaré sphere and φ is the azimuthal angle. This equation shows how a point on the complex plane is related to a point on the Poincaré sphere, with θ and φ describing the polarization state. The north and south poles of the Poincaré sphere ($\theta = 0$ and $\theta = \pi$, respectively) correspond to right and left circular polarizations, while points on the equator ($\theta = \pi/2$) represent linear polarizations (see figure 1(a)). The remaining points represent elliptical polarizations, with the azimuthal angle φ indicating the orientation of the ellipse.

Let us consider the action of a waveplate on an arbitrarily polarized plane wave (1). Note that a similar consideration is applicable to the case depicted in figure 1(b), where a nanostructure with, for example, C_{2v}, C_{1h} or D_{2h} symmetry plays the role of a conventional waveplate made from a uniaxial crystal. From the modal perspective, this happens because the orthogonal eigenmodes, even and odd with respect to the mirror-symmetry plane, are non-degenerate, and excited with different phases, depending on their resonant frequencies [37, 38]. First we consider the case where the waveplate is oriented with its slow axis along the x-direction. As such, it just provides an additional phase δ between

the components of the input Jones vector $\mathbf{E} = (E_x, E_y)^\top$. For convenience, we write the new vector as $\tilde{\mathbf{E}} = (E_x e^{\mathrm{i}\,\delta/2}, E_y e^{-\mathrm{i}\,\delta/2})^\top$. Using the following relations

$$E_R = \frac{E_x - \mathrm{i}\,E_y}{\sqrt{2}}, \quad E_L = \frac{E_x + \mathrm{i}\,E_y}{\sqrt{2}}, \tag{6}$$

$$E_x = \frac{E_R + E_L}{\sqrt{2}}, \quad E_y = -\frac{E_R - E_L}{\mathrm{i}\,\sqrt{2}}, \tag{7}$$

we obtain new values $\tilde{E}_L$ and $\tilde{E}_R$ after the waveplate:

$$\begin{pmatrix} \tilde{E}_R \\ \tilde{E}_L \end{pmatrix} = \begin{pmatrix} \cos\delta/2 & \mathrm{i}\,\sin\delta/2 \\ \mathrm{i}\,\sin\delta/2 & \cos\delta/2 \end{pmatrix} \begin{pmatrix} E_R \\ E_L \end{pmatrix} = (\mathbb{I}\cos\delta/2 + \mathrm{i}\,\sigma_x \sin\delta/2) \begin{pmatrix} E_R \\ E_L \end{pmatrix}. \tag{8}$$

Here σ_x is one of the Pauli matrices

$$\sigma_x = \begin{pmatrix} 0 & 1 \\ 1 & 0 \end{pmatrix}, \quad \sigma_y = \begin{pmatrix} 0 & -\mathrm{i} \\ \mathrm{i} & 0 \end{pmatrix}, \quad \sigma_z = \begin{pmatrix} 1 & 0 \\ 0 & -1 \end{pmatrix}. \tag{9}$$

From (8), one can note that if the phase shift corresponds to half-wave retardation, $\delta = \pi$, we have perfect conversion between cross-polarized fields: $E_L \to \mathrm{i}\,E_R$, $E_R \to \mathrm{i}\,E_L$.

Let us check what happens if we rotate the optical axis of a waveplate, so as to form an angle β with the x-axis. We provide the derivations for this case in appendix C. Eventually, we get the general formula for a plane wave transmitted through a waveplate with arbitrary retardance δ (or a nanostructure with 2-fold rotational symmetry):

$$\begin{pmatrix} \tilde{E}_R \\ \tilde{E}_L \end{pmatrix} = \left(\mathbb{I}\cos\delta/2 + \mathrm{i}\,\left(\cos 2\beta\sigma_x + \sin 2\beta\sigma_y\right)\sin\delta/2\right) \begin{pmatrix} E_R \\ E_L \end{pmatrix}. \tag{10}$$

Importantly, we see that transformation (10) is performed via an $SU(2)$ matrix. One can indeed easily check that the determinant of this matrix is equal to 1, and $U^\dagger U = 1$. For a waveplate rotated by the angle $\beta = 45°$ we get

$$\begin{pmatrix} \tilde{E}_R \\ \tilde{E}_L \end{pmatrix} = (\mathbb{I}\cos\delta/2 + \mathrm{i}\,\sigma_y \sin\delta/2) \begin{pmatrix} E_R \\ E_L \end{pmatrix}. \tag{11}$$

In this case for $\delta = \pi$ we have $E_R \to -E_L$, $E_L \to E_R$, with a different relative phase compared to the case above ($\beta = 0$). From equation (10) one can see that a plane wave transmitted through a half-wave plate rotated by an angle β is transformed as follows

$$\begin{pmatrix} \tilde{E}_R \\ \tilde{E}_L \end{pmatrix} = \begin{pmatrix} 0 & \mathrm{i}\,e^{-2\mathrm{i}\beta} \\ \mathrm{i}\,e^{2\mathrm{i}\beta} & 0 \end{pmatrix} \begin{pmatrix} E_R \\ E_L \end{pmatrix} \tag{12}$$

Let us note that in the general case, the $SU(2)$ transformation looks as follows

$$\begin{pmatrix} \tilde{E}_R \\ \tilde{E}_L \end{pmatrix} = \left[\mathbb{I}\cos\frac{\delta}{2} + \mathrm{i}\,\left(n_x\sigma_x + n_y\sigma_y + n_z\sigma_z\right)\sin\frac{\delta}{2}\right] \begin{pmatrix} E_R \\ E_L \end{pmatrix}, \qquad n_x^2 + n_y^2 + n_z^2 = 1. \tag{13}$$

Interestingly, by comparing equations (10) and (13), one can see that a waveplate cannot realize a rotation about the z-axis (generated by σ_z). Such a rotation, however, can be achieved using a gyrotropic medium [4, 39, 40]. The group $SU(2)$ is the double cover (indeed, the universal covering group) of $SO(3)$, the group of all proper rotations in three dimensions (orthogonal transformations with unit determinant) [34, 41]. In the present context, these are rotations of the Poincaré sphere [42, 43]. This means that actually two $SU(2)$ matrices correspond to each rotation of the Poincaré sphere. One can check that during any transformation of the form (10), all points of the Poincaré sphere are just rotated around some horizontal axis (the orientation of the axis depends on β). For this, one should keep in mind the relation between Stokes parameters and Jones matrices [44, 45] and compare with Chapter IV.5 '$SU(2)$: Double Covering and the Spinor' in [41]. For convenience, we restrict our attention to the evolution of an initially circularly polarized state $|R\rangle$. The path of this state under action of a waveplate is drawn in figure 1(a). Depending on the retardance δ of the waveplate, the path may have different lengths and can therefore be parametrized by δ. Using (12) it is easy to see that the phases of the final state $|L\rangle$ will be different, and β- dependent. For two different paths that cut out a slice (a closed contour) from the sphere, the phase difference will be equal to the half of the solid angle $\Omega/2$ [2].

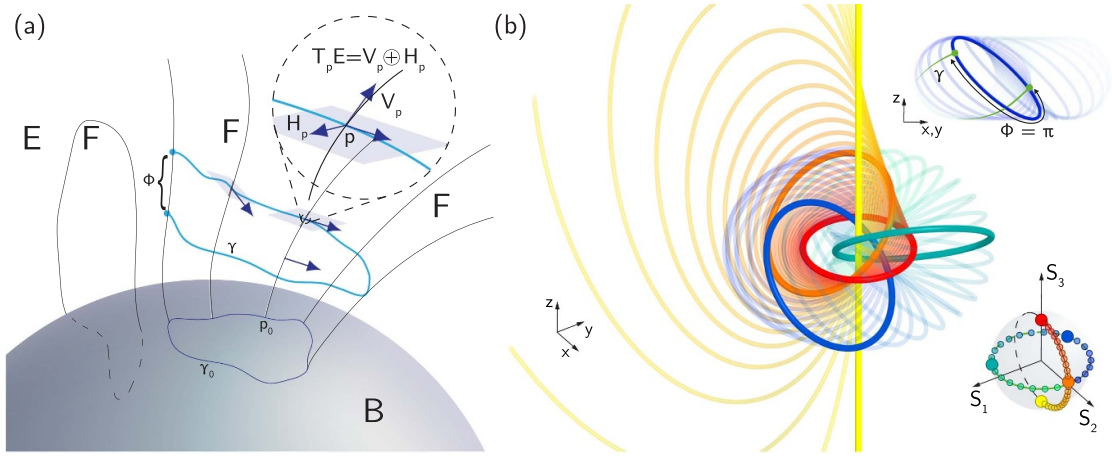


Figure 2. (a) Illustration of a circle bundle over the sphere S^2. Fibres F are topologically circles S^1, the base manifold is a sphere S^2. The horizontal lift γ of the curve γ_0 via a connection is shown. The tangent space to the total space E at a point $p \in E$, T_pE is shown, together with its decomposition as the direct sum of a horizontal and vertical subspace. Horizontal subspaces are determined by a connection form. The holonomy Φ of the connection is the geometric phase. Physically, a point on the base sphere represents the polarization state, the fibre coordinate represents the common optical phase, and Φ is the phase accumulated after a closed polarization cycle. (b) Visualization of the Hopf fibration. The three-dimensional sphere S^3 is fibred into circles and depicted in 3D space via stereographic projection. The circles are mapped to polarization states on the Poincaré sphere S^2. The correspondence is indicated by colours; for example, the orange circle on S^3 is mapped to the orange point on S^2. The inset in the upper right shows one of the possible horizontal lifts of the closed path along the equator of S^2, resulting in a holonomy of π.

Figure 1(c) shows the numerically calculated geometric phase for a cuboid nanoparticle in air (D_{2h}) illuminated by an RCP fundamental Gaussian beam with $m = 1$ and $l = p = 0$ (see also appendix G). The cross-polarized component (LCP, $m = -1$) acquires a phase factor $e^{2i\beta}$, so its phase winds by 2π as the particle is rotated from $\beta = 0$ to $\beta = \pi$. In the Poincaré-sphere representation, the corresponding $SU(2)$ rotation axis simultaneously completes one full circuit of the equator. The phase of the co-polarized component ($m = 1$) is independent of β.

We should note that the analogy between a half-wave plate and a nanostructure is not perfect. In the case of a non-reflective wave plate, we have a well-defined path parametrizing the polarization state of a propagating wave, which can be depicted on the Poincaré sphere. In the case of a single nanostructure, it is not clear what exactly should be considered as a state, nor whether it can be parametrized by a distance. Moreover, as discussed in [46–48], the question of cross-conversion efficiency should also be taken into account. One could consider the fields inside the nanostructure and only the polarization state of the forward-propagating wave component, but this seems somewhat unnatural. However, assuming equal amplitudes of the two excited eigenmodes, one can still formally write the same $SU(2)$ transformation.

2.2. Differential geometric viewpoint

Let us now consider the simple experiment discussed above from a differential geometric point of view. For the basic definitions, one may also consult [49–51]. In general, when the polarization state on the Poincaré sphere (S^2) traverses a closed path, the actual state of light (including the common phase) traces a path in another, higher-dimensional space (see figure 2(a)) which, in our specific case, is given by the three-dimensional sphere S^3. This corresponds to the two normalized complex numbers in equation (3). In this space, the path is not necessarily closed; its behaviour is in fact determined by the specific way in which the point moves, physically via a waveplate and mathematically through the *holonomy* of a connection [51–53] — measuring the extent to which the path fails to close —which actually represents the geometric phase. The three-dimensional sphere is fibred into circles (corresponding to the total phase). Each circle is mapped to a single point of the base sphere S^2 under the bundle projection. Note, that in the figure 2(a), the fibres are shown as attached to S^2 only schematically, the base sphere S^2 should not be interpreted as an embedded submanifold of the total space S^3.

This construction corresponds to the so-called Hopf fibration. In the same way as a two-dimensional sphere S^2 may be mapped onto a two-dimensional plane (appendix A), a three-dimensional sphere may be mapped onto a three-dimensional space. Due to the properties of stereographic projection, circles are mapped to circles or straight lines. Figure 2(b) visualizes the Hopf bundle through a stereographic projection for a set of polarization states on the Poincaré sphere. The colours indicate the correspondence

between the fibres and the polarization states shown in the inset. Points lying at the same latitude are mapped to circles of equal radius, which form a torus. Some intuition can be also gained from specifically dedicated videos, see e.g. [36, 54].

2.2.1. Fibre bundles

When we forget the total phase and consider only the polarization, we have a point on the Poincaré sphere. This sphere will be called a base space. The total phase (we could deal with the amplitude as well, but we shall not do this here) can be depicted as a point on a circle S^1. Thus, to each point on the Poincaré sphere there corresponds a circle, accommodating the total phase. The whole system is a fibre bundle, with a total space E, base space $B = S^2$ and fibre $F = S^1$ (see figure 2(a)) [50, 51]. We denote this arrangement as (E, B, π, F). Here $\pi\colon\ E \to B$ is the projection that maps each fibre F_x, $x \in B$, to the point x itself. We will discuss the structure of the total space E in our case in detail later on. So we can imagine the circles as being 'attached' to the sphere, as the teeth of a comb are attached to its base. However, this analogy should not be understood literally: the circles are associated with the points of the sphere through the mapping π, rather than physically attached to or embedded in the sphere.

We will work with locally trivial fibre bundles, i.e. those obtained by appropriately 'gluing' trivial bundles (E, U, π, F) with $E = U \times F$, where $U \subseteq B$ is an open set from an open cover of B and $\pi\colon\ E \to U$ is the projection onto U; that is, for $(x, f) \in U \times F$, $\pi(x, f) = x$. The detailed construction of a locally trivial fibre bundle is not essential for our purposes; it suffices to know that our bundle is 'good enough'.

2.2.2. Connections

However, since there is no canonical way to identify the fibres with each other, we need an additional structure, a *connection*, that specifies how neighbouring fibres are 'glued together'. For this purpose, we introduce horizontal and vertical subspaces of the tangent space T_pE to some point p of the total space E.

The **vertical subspace** V_p is the subspace of the tangent space T_pE that consists of vectors that are tangent to the fibres. Formally, it is defined as:

$$V_p = \left\{ u \in T_pE \,|\, \pi_* u = 0 \right\}, \tag{14}$$

where $\pi\colon\ E \to B$ is the projection map, and $\pi_* u$ denotes the pushforward of u, recalled below.

Pushforward: let $f\colon\ M \to N$ be a smooth map between manifolds M and N. The differential, or pushforward of f, denoted by f_*, is a map

$$f_*\colon\ T_pM \to T_{f(p)}N \tag{15}$$

between the tangent spaces T_pM and $T_{f(p)}N$, mapping a vector $v \in T_pM$ to a vector $f_* v \in T_{f(p)}N$. Informally, if some vector v is a tangent vector to a particular curve $\mathcal{C}$ in M passing through p, then, after a pushforward, it becomes $f_* v$, a tangent vector at $f(p)$ to the image curve $f(\mathcal{C})$. The **horizontal subspace** H_p at a point p in the bundle E is a subspace of the tangent space T_pE that complements the vertical space. The term 'horizontal' should not be understood as implying orthogonality to the vertical subspace, as no metric has been introduced so far. A **connection** on a bundle (E, B, π, F) can be described in terms of a connection form $\mathcal{A}$. The **connection form** $\mathcal{A}$ is a 1-form on E whose value specifies the vertical component of a tangent vector. Its action on a tangent vector $u \in T_pE$ is given by:

$$\mathcal{A}_p(u) := \mathrm{i}\, a, \qquad \mathrm{ver}\, u = a\, u_v \in V_p, \quad a \in \mathbb{R}. \tag{16}$$

where $\mathrm{ver}\, u$ denotes the vertical component of u, and u_v is the vertical vector field written explicitly in equation (29). Thus, $\mathcal{A}_p(u)$ is a purely imaginary number whose real coefficient a specifies the vertical component of u. Concretely, this 1-form just takes a vector from the tangent space T_pE and returns its projection onto the vertical subspace V_p, namely the component tangent to the fibre. Equivalently, a connection specifies a complement H_p to the vertical subspace V_p and picks up the vertical component of a vector in T_pE: in other words, it is the (oblique) projection onto V_p along H_p. Explicitly, the **horizontal subspace** is defined as follows:

$$H_p = \left\{ u \in T_pE \,|\, \mathcal{A}_p(u) = 0 \right\}.$$

Vertical and horizontal components are depicted in figure 2(a). The definitions above were quite general, but for the physical problems under consideration here, we are basically interested in the celebrated

Hopf bundle, to be discussed below. Physically, this condition fixes the choice of a common phase while the polarization changes. For the connection used here, horizontal transport means that infinitesimally neighbouring states are in phase in the Pancharatnam sense, see appendix H.

2.2.3. Geometry of the Hopf bundle

We shall illustrate the above general scheme in the important specific case provided by the Hopf bundle, shortly $\mathscr{H}$, following [50]. The total space in this case is a three-dimensional sphere S^3, embedded in the four-dimensional space $\mathbb{C}^2$, as

$$|z_1|^2 + |z_2|^2 = 1. \tag{17}$$

The base space is the two-dimensional sphere S^2. The projection map $\pi : S^3 \to S^2$ reads

$$\pi(z_1, z_2) = \left(2\,\mathrm{Re}\,(z_1\overline{z_2}),\ 2\,\mathrm{Im}\,(z_1\overline{z_2}),\ |z_1|^2 - |z_2|^2\right) = (x, y, z). \tag{18}$$

These expressions for the three components resemble the Stokes parameters (with a change in notation), and this is not a coincidence. One can check that, actually, $x^2 + y^2 + z^2 = 1$. Note that

$$\pi(z_1, z_2) = \pi\left(\mathrm{e}^{\mathrm{i}\,\alpha} z_1, \mathrm{e}^{\mathrm{i}\,\alpha} z_2\right), \tag{19}$$

The fibre F is the circle $S^1 \approx U(1)$ (that is, we have a *principal bundle* with *structure group* $G = U(1)$) and the above formula says that the projection is invariant under the action of $U(1)$ group. Thus, points on the same fibre have identical polarization and differ only by the common optical phase. In other words, the point on the base sphere is determined by the Stokes parameters, whereas motion along the $U(1)$ fibre leaves these parameters unchanged.

Let us now define a 'canonical' connection. Let $\langle\cdot,\cdot\rangle : \mathbb{C}^2 \times \mathbb{C}^2 \to \mathbb{C}$ be the standard Hermitian inner product in $\mathbb{C}^2$. For any $(z_1, z_2), (w_1, w_2) \in \mathbb{C}^2$, it is defined as:

$$\langle (z_1, z_2), (w_1, w_2) \rangle := \bar{z}_1 w_1 + \bar{z}_2 w_2. \tag{20}$$

Let us consider a point $p \in S^3$ and take any vector $v \in T_p S^3$. If $p \in S^3$ corresponds to $(z_1, z_2) \in \mathbb{C}^2$, then the vertical space V_p is defined as

$$V_p = \{(\mathrm{i}\ a z_1, \mathrm{i}\ a z_2) \mid a \in \mathbb{R}\} \tag{21}$$

For the horizontal space, we take

$$H_p = \left\{(w_1, w_2) \in \mathbb{C}^2 \mid \langle (z_1, z_2), (w_1, w_2) \rangle = 0\right\}. \tag{22}$$

That is, H_p consists of all vectors tangent to S^3 at p that are orthogonal to p when p is viewed as a radius-vector in $\mathbb{C}^2$. One can define the connection 1-form $\mathcal{A}$ on S^3 as follows:

$$\mathcal{A} = 2g\,(\bar{z}_1\,\mathrm{d}z_1 + \bar{z}_2\,\mathrm{d}z_2), \tag{23}$$

where g is a scaling factor. Indeed, action of a form on arbitrary complex vector (v_1, v_2) returns its vertical component:

$$2g\,(\bar{z}_1\,\mathrm{d}z_1 + \bar{z}_2\,\mathrm{d}z_2)\,(v_1, v_2) = 2g\,(\bar{z}_1 v_1 + \bar{z}_2 v_2) \tag{24}$$

For the standard Hopf normalization $g = 1/2$ (compare with (20)). We will keep this factor to generalize our considerations later on. Expanding the connection form in terms of real and imaginary parts, we get

$$\mathcal{A} = 2g\,\mathrm{Re}\,(\bar{z}_1\,\mathrm{d}z_1 + \bar{z}_2\,\mathrm{d}z_2) + 2\mathrm{i}\ g\,\mathrm{Im}\,(\bar{z}_1\,\mathrm{d}z_1 + \bar{z}_2\,\mathrm{d}z_2). \tag{25}$$

However, since $(z_1, z_2) \in S^3$, and (17), we have

$$2\,\mathrm{Re}\,(\bar{z}_1\,\mathrm{d}z_1 + \bar{z}_2\,\mathrm{d}z_2) = \mathrm{d}\left(|z_1|^2 + |z_2|^2\right) = 0, \tag{26}$$

and thus,

$$\mathcal{A} = 2\mathrm{i}\ g\,\mathrm{Im}\,(\bar{z}_1\,\mathrm{d}z_1 + \bar{z}_2\,\mathrm{d}z_2). \tag{27}$$

Finally, expanding $z_1 = x_1 + \mathrm{i}\, x_2$, and $z_2 = x_3 + \mathrm{i}\, x_4$ we can express $\mathcal{A}$ as

$$\mathcal{A} = 2\mathrm{i}\, g\,(x_1\,\mathrm{d}x_2 - x_2\,\mathrm{d}x_1 + x_3\,\mathrm{d}x_4 - x_4\,\mathrm{d}x_3)\,, \tag{28}$$

where x_i represent the real components of the vector in $\mathbb{R}^4$.

Let us illustrate the action of this form in coordinates and consider the vertical and horizontal subspaces for the particular example of the Hopf fibration. Consider, at $p = (z_1, z_2) \in S^3$, the following orthonormal basis of tangent vectors to S^3:

$$u_v = -x_2\partial_1 + x_1\partial_2 - x_4\partial_3 + x_3\partial_4, \tag{29}$$

$$u_{h1} = -x_3\partial_1 + x_4\partial_2 + x_1\partial_3 - x_2\partial_4,$$

$$u_{h2} = -x_4\partial_1 - x_3\partial_2 + x_2\partial_3 + x_1\partial_4, \tag{30}$$

where a physicist can think about ∂_i as unit basis vectors $\partial_i \leftrightarrow \mathbf{e}_i$ (in this particular case). Then, for a vector u_v starting at $p = (x_1, x_2, x_3, x_4)$ and ending at

$$h(t) = (x_1 - tx_2, x_2 + tx_1, x_3 - tx_4, x_4 + tx_3)\,, \tag{31}$$

we obtain

$$h(t) - p = (1 + \mathrm{i}\, t)p - p = (\mathrm{i}\, tz_1, \mathrm{i}\, tz_2)\,. \tag{32}$$

which means that this vector indeed belongs to the vertical space (21). Otherwise, one can directly write the action of the 1-form (28) on (29): Using that $\mathrm{d}x_j(\partial_k) = \delta_{jk}$, we have:

$$\mathcal{A}(u_v) = 2\mathrm{i}\, g\left(x_1^2 + x_2^2 + x_3^2 + x_4^2\right) = 2\mathrm{i}\, g, \tag{33}$$

since the point lies on the unit 3-sphere. For completeness, one can also verify that for the two other tangent vector fields (30) the form gives

$$\mathcal{A}(u_{h1}) = \mathcal{A}(u_{h2}) = 0, \tag{34}$$

which confirms that only u_v has a nonzero projection on the vertical subspace, and u_{h1} and u_{h2} are horizontal vector fields.

2.2.4. Horizontal lift and holonomy

In this section, we introduce the definitions that are likely the most important for understanding the Berry phase. Let (E, B, π, F) be a smooth fibre bundle, where E is the total space (S^3 in our case), B is the base space (Poincaré sphere S^2 in our case), $\pi\colon E \to B$ is the projection map, and F is the fibre. Let $v \in T_xB$ be a tangent vector at $x \in B$, and let $p \in E$ be a point such that $\pi(p) = x$. The **horizontal lift** of some vector v at p is the unique vector $\tilde{v} \in T_pE$ satisfying the following conditions:

1. Projection preservation: the vector $\tilde{v}$ projects to v under the pushforward of π, i.e.

$$\pi_*(\tilde{v}) = v, \tag{35}$$

   where $\pi_*\colon T_pE \to T_xB$.

2. Horizontality: the vector $\tilde{v}$ lies in the horizontal subspace $H_p \subset T_pE$, defined by the connection form $\mathcal{A}$, i.e.

$$\mathcal{A}_p(\tilde{v}) = 0. \tag{36}$$

   The *horizontal lift* γ *of a curve* γ_0 on the base space is defined as follows: the projection of a lifted curve should be the initial curve, and its tangent vector should be the horizontal lift of the tangent vector to the initial curve. In figure 2 the horizontal lift of the curve on the base space is depicted with light blue as well as lifts of tangent vectors. In appendix C.1 we provide an example in coordinates.

However, if the path on the base space is closed, the lifted path, in general, is not closed: one arrives at a different point on the fibre, as shown in the figure. This difference is called **holonomy** of the connection, and corresponds exactly to the geometric phase [26, 55]! An example is also given in appendix C.1. Optically, the polarization may therefore return to its initial state while the field acquires a

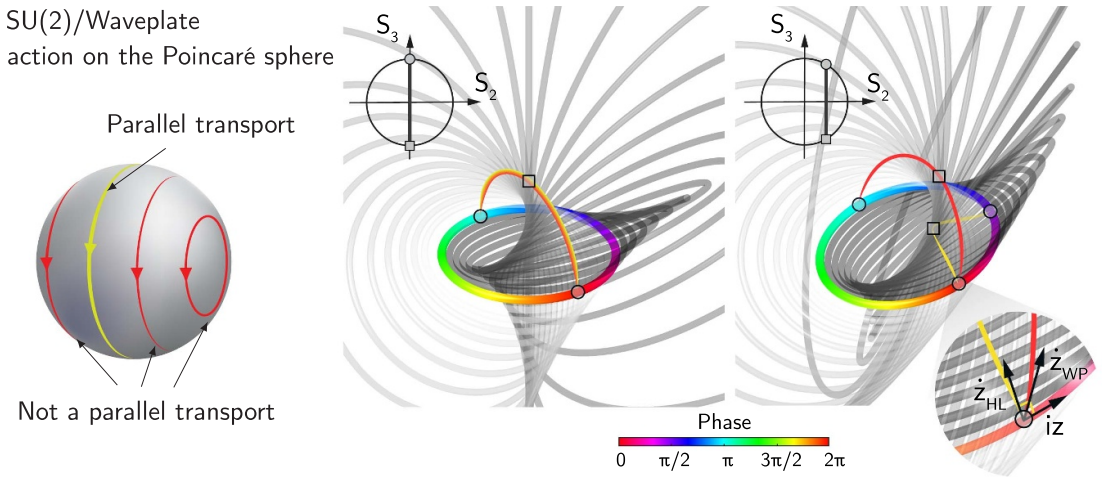


Figure 3. Waveplate evolution and parallel transport in the Hopf bundle. Left: trajectories on the Poincaré sphere generated by $U(\delta) = \exp(\mathrm{i}\,\delta\sigma_y/2)$. Rotation about S_2 produces a great circle for $S_2 = 0$ and small circles for $S_2 \neq 0$. Right: stereographic representations of the corresponding Hopf fibres and lifted trajectories. The waveplate evolution (WP, red) coincides with the horizontal lift (HL, yellow) for the great circle, whereas the two lifts differ for small circles, reflecting a nonzero dynamical phase. The highlighted fibre is coloured by the global phase relative to the initial Jones state. The enlarged view illustrates the local distinction between horizontal transport and waveplate evolution.

nonzero phase, which can be measured relative to a reference field. In principle, holonomy can be introduced prior to the notion of curvature, but the latter notion is crucial for both theoretical and computational purposes.

The last definition is that of *parallel transport*: given a point $p \in E$, this is simply the motion of this point along a horizontally lifted curve. We briefly elaborate on the above concepts in appendix C.3.

2.2.5. Action of the waveplate

As we have seen earlier, the action of the waveplate is described with the help of the $SU(2)$ matrix (10). But how can we see that this action corresponds somehow to the connection form (28)? We discuss this in detail in the appendix D. The answer is the following: the motion of a point on the sphere S^3 under the action (10) of an $SU(2)$ one-parameter subgroup comes from parallel transport if and only if the corresponding projection on the Poincaré sphere moves along a great circle, namely, a geodesic on S^2 [4, 56–58]. We illustrate this schematically in figure 3. Paths on the stereographic projections of the parts of the Hopf fibration illustrate the distinction between the waveplate-induced lift and the horizontal lift. One can note that both project onto the same curve γ_0 on the Poincaré sphere, but the horizontal-lift tangent is horizontal by definition, whereas the waveplate-induced tangent need not be horizontal. For the great-circle trajectory $S_2 = 0$, the waveplate-induced tangent at point z lies in H_z, and the waveplate evolution therefore coincides with parallel transport. For the small-circle trajectories $S_2 \neq 0$, it also has a nonzero component in V_z, along the fibre direction $u_v(z) = \mathrm{i}\,z$. The enlarged inset illustrates this distinction at the common initial point $\mathcal{A}_z(\dot{z}_{\mathrm{HL}}) = 0$, whereas $\mathcal{A}_z(\dot{z}_{\mathrm{WP}}) \neq 0$. After a closed circuit on the base sphere, the endpoint displacement of the horizontal lift along the initial fibre gives the holonomy, and hence the geometric phase. The waveplate-induced lift additionally accumulates a dynamical phase associated with its vertical component.

3. A direct Pancharatnam–Berry-phase analogy for vortex beams via the Poincaré sphere

Let us now consider vortex beams. In cylindrical coordinates, vortex beams allow for the construction of a higher-order Poincaré sphere [15, 59], which is fully analogous to the usual one:

$$|R_m\rangle \sim \mathrm{e}^{\mathrm{i}m\varphi}\,(\hat{\boldsymbol{\rho}} + \mathrm{i}\,\hat{\boldsymbol{\varphi}})\,, \tag{37}$$

$$|L_m\rangle \sim \mathrm{e}^{-\mathrm{i}m\varphi}\,(\hat{\boldsymbol{\rho}} - \mathrm{i}\,\hat{\boldsymbol{\varphi}})\,, \tag{38}$$

where $|R_m\rangle$ and $|L_m\rangle$ signify right- and left-handed vortex beams, respectively, with $m \in \mathbb{Z}$ denoting the TAM projection, φ the azimuthal angle, and $\hat{\boldsymbol{\rho}}$, $\hat{\boldsymbol{\varphi}}$ are unit vectors of cylindrical coordinate system. The equivalence sign $\sim$ stands for the symmetry behaviour, i.e. behaviour under rotations around the z-axis.

Precisely, this means that under rotation of the vector function as a whole by some angle α around the z-axis, the function does not change except for an additional phase $e^{\pm im\alpha}$. See e.g. [60, 61] for a precise definition; a detailed discussion can be found in [62]. Note, that

$$(\hat{\mathbf{x}} \pm i\,\hat{\mathbf{y}}) = e^{\pm i\varphi}\,(\hat{\boldsymbol{\rho}} \pm i\hat{\boldsymbol{\varphi}})\,, \tag{39}$$

and the sign refers to the polarization (helicity) here. We omit the dependence on the radial coordinate r [63], since it does not alter the general symmetry we are interested in. Similarly to equation (1) we can introduce the following linear combination, or a vector vortex beam:

$$\mathbf{E} = c_1|R_m\rangle + c_2|L_m\rangle. \tag{40}$$

At this stage we want to describe an experiment, what would be analogous to the one with the waveplate. A vector vortex beam is fundamentally different from a plane wave, being anisotropic in the transverse direction. As already discussed, for plane waves, not only waveplates but also geometric-phase metasurfaces with cuboid dielectric metaatoms are widely used [64, 65]. Related PB elements based on subwavelength dielectric gratings and patterned liquid crystals were demonstrated in [11, 66], see also the review [2].

Such metasurfaces, as well as liquid-crystal-based setups governed by the same principles, are often used for structured-light generation [11, 67]. Indeed, each metaatom has, e.g. C_{2v}, D_{2h} or C_{1h} symmetry. For these symmetries, two eigenmodes, one of which is excited by an x-polarized wave and the other by an y-polarized wave, are transformed according to the different irreducible representations, and, as a consequence, have different resonance frequencies and are excited with different phases [37, 62]. This consideration via the eigenmodes and irreps may appear too complicated for this simple case of a rectangular block; however, it can be easily adapted to the vortex beam case. We expand the discussion on the modal excitation in the appendix E. Indeed, vector beams, which are defined as:

$$|\mathrm{B}_{me}\rangle \propto |L_m\rangle + |R_m\rangle \tag{41}$$

$$|\mathrm{B}_{mo}\rangle \propto |L_m\rangle - |R_m\rangle, \tag{42}$$

where the indexes e and o denote the parity under reflection in the $y = 0$ plane, refer to the endpoints of a diameter of the higher-order Poincaré sphere. They serve as an analogy for vertical and horizontal linear polarization in the plane wave case. Thus, instead of the rectangular block, one should use a nanostructure, in which $|\mathrm{B}_{me}\rangle$ and $|\mathrm{B}_{mo}\rangle$ are transformed according to the different irreps. This metaatom should have $C_{\mathfrak{n}v}$ or $D_{\mathfrak{n}h}$ symmetry with $2m = \mathfrak{n}\nu, \quad \nu \in \mathbb{Z}$ (See also [62], section 8). For such a structure, these vector beams will excite eigenmodes which have different phases, leading to exactly the same process previously discussed. Note that this process is not perfect because other values of m are also obtained during scattering. Since one cannot avoid them, the only way out is to tailor the geometry so as to minimize their contribution. Although this process is analogous to the simplest case, there is an important difference. In order to obtain the same phase difference δ one should rotate the nanostructure by a smaller angle β (compare figure 1(a) and 4(a)). One can also notice that opposite points on the diameter refer to the beam rotation by $\beta = \pi/(2m)$, as well as the nanostructure rotation for the opposite paths on the Poincare sphere. For a plane wave $m = \pm 1$. It is also analogous to the transformation implemented by a q-plate, as described in [67, 68]. Although the physical implementations are different, the detailed shape of the q-plate is not essential for this analogy.

Let us also note that, in principle, if we have an incident wave with TAM projection m^{inc} and an output wave of the same frequency with the TAM projection m^{out}, the acquired phase will be equal to [69]

$$\phi(\beta) = \left(m^{\mathrm{inc}} - m^{\mathrm{out}}\right)\beta, \tag{43}$$

however, the corresponding geometric interpretation is not straightforward for other $|m^{\mathrm{out}}| \neq |m^{\mathrm{inc}}|$. Moreover, in view of the selection rules for scattering, only $m^{\mathrm{out}} = m^{\mathrm{inc}} + \mathfrak{n}\mathbb{Z}$ are allowed.

Figure 4(b) shows a numerical calculation of geometric phase for particles of different symmetries illuminated by a beam with $m = 3$ featuring second order phase singularity (LG mode with $l = 2$, $p = 0$, see appendix G). One can see that both D_{3h} and D_{6h} particles with the same input, provide a 2π phase winding of the cross polarized component under rotation by the angle $\pi/3$. In summary, the construction is the direct analogue of the polarization case, with the two opposite-TAM states replacing the two circular-polarization states and the rotation of the nanostructure controlling the acquired phase.

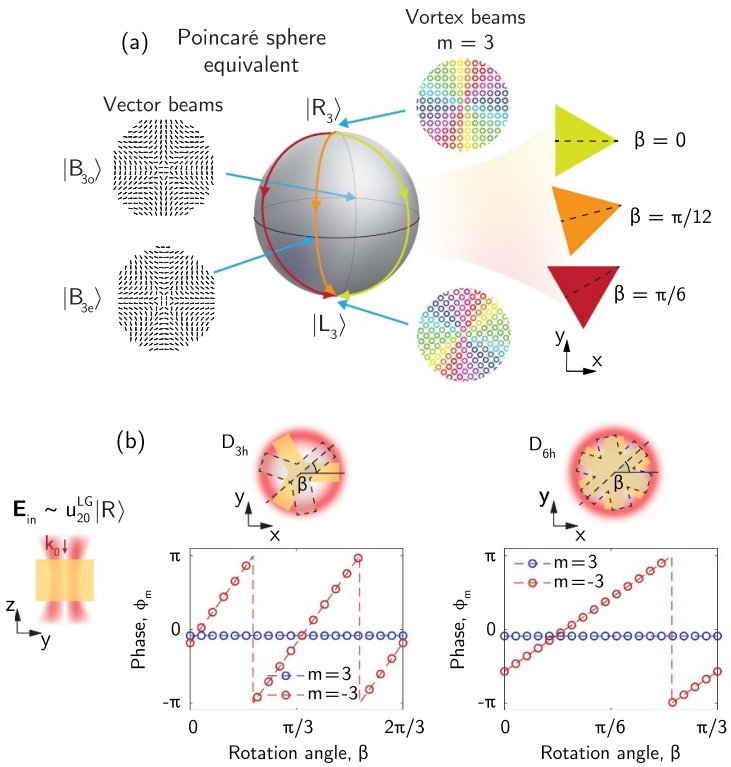


Figure 4. (a) Geometry of the experiment involving the transmission of vortex beams with TAM projection m through a prism with n-fold rotational symmetry. This setup is fully analogous to the one depicted in figure 1, but different β is required. (b) Numerically calculated phase acquired by the rotation of nanoparticles with D_{3h} and D_{6h} symmetries under excitation by a vortex beam ($m = 3$). The phase is wrapped to the range $[-\pi, \pi]$, circular markers indicate the calculated points, the dashed lines are guides to the eye. For both nanoparticles the condition $2m = n\nu$ is satisfied, therefore 2π phase is accumulated by $\pi/3$ rotation.

4. The usual geometric phase of vortex beams via the Hermite–Gaussian sphere

Let us now proceed to another experiment, which is commonly associated with the geometric phase of optical beams. This experiment possesses a completely different geometry, when compared to the one described above. First, we consider only the scalar part of the beam, because polarization may be considered independently for this experiment. Here we will use the paraxial approximation. In the previous case, no such approximation was needed. The Hermite–Gaussian modes are solutions of the paraxial wave equation [70–72]

$$\frac{\partial^2}{\partial x^2}u(\mathbf{r}) + \frac{\partial^2}{\partial y^2}u(\mathbf{r}) = -2\mathrm{i}\,k\frac{\partial}{\partial z}u(\mathbf{r}), \tag{44}$$

and may be written as

$$u^{\mathrm{HG}}_{\nu\eta}(\mathbf{r}) = \frac{1}{\gamma}\psi_\nu\left(\frac{x}{\gamma}\right)\psi_\eta\left(\frac{y}{\gamma}\right)\exp\left[\frac{\mathrm{i}\,kr_t^2}{2R} - \mathrm{i}\,\chi\,(\nu+\eta+1)\right], \tag{45}$$

where $\psi_n(\xi)$ are the normalized Hermite functions corresponding to the one-dimensional harmonic oscillator:

$$\psi_n(\xi) = \frac{1}{\sqrt{2^n n!\sqrt{\pi}}}\,\mathrm{e}^{-\xi^2/2}H_n(\xi). \tag{46}$$

$\chi = \chi(z)$ is the Gouy phase, $\gamma = \gamma(z)$ is the spot radius and $R = R(z)$ is the radius of the curvature of the wavefront, $\eta, \nu \in \mathbb{N}_0$, k is a wavenumber, $r_t^2 = x^2 + y^2$, $H_n(\xi)$ is a Hermite polynomial [71]. The solutions can be also presented in a different form:

$$u^{\mathrm{LG}}_{\ell p}(\mathbf{r}) = \exp\left[\frac{ik}{2R}r_t^2 - \mathrm{i}\,\chi\,(N+1)\right]\frac{1}{\gamma}\psi_{lp}\left(\frac{r_t}{\gamma}, \varphi\right), \tag{47}$$

$$\psi_{\ell p}(\rho,\varphi)=\sqrt{\frac{p!}{\pi\,(p+|\ell|)!}}\,\mathrm{e}^{-\rho^2/2}\,\mathrm{e}^{\mathrm{i}\,\ell\varphi}\,\rho^{|\ell|}\,L_p^{|\ell|}\left(\rho^2\right), \tag{48}$$

where $N=\eta+\nu=2p+|\ell|$ and $L_p^{|\ell|}$ is the generalized Laguerre polynomial. Notice that there are $N+1$ solutions for each N. For our purposes, an exact form is not necessary, because we are only interested in the following presentation [71, 73, 74]:

$$u_{\nu\eta}^{\mathrm{HG}}(\mathbf{r})=\frac{1}{\sqrt{\nu!\eta!}}\left(\hat{a}_x^\dagger\right)^\nu\left(\hat{a}_y^\dagger\right)^\eta u_{00}(\mathbf{r}) \tag{49}$$

where

$$\hat{a}_x=\frac{1}{\sqrt{2bk}}\left[kx+(b+\mathrm{i}\,z)\frac{\partial}{\partial x}\right], \tag{50}$$

$$\hat{a}_x^\dagger=\frac{1}{\sqrt{2bk}}\left[kx-(b-\mathrm{i}\,z)\frac{\partial}{\partial x}\right]. \tag{51}$$

and $\hat{a}_y$ is defined analogously with $x\to y$ [71, 73], b is the Rayleigh range, $\chi(z)=\arctan(z/b)$, and $\frac{1}{b+\mathrm{i}\,z}=\frac{1}{k\gamma^2}-\frac{\mathrm{i}}{R}$ [71]. Let us define the operators [75–77]

$$L_x=\frac{1}{2}\left(\hat{a}_x^\dagger\hat{a}_x-\hat{a}_y^\dagger\hat{a}_y\right)=\frac{1}{4bk}\left[k^2\left(x^2-y^2\right)+2\mathrm{i}\,kz\left(x\partial_x-y\partial_y\right)-\left(b^2+z^2\right)\left(\partial_x^2-\partial_y^2\right)\right]. \tag{52}$$

$$L_y=\frac{1}{2}\left(\hat{a}_x^\dagger\hat{a}_y+\hat{a}_y^\dagger\hat{a}_x\right)=\frac{1}{2bk}\left[k^2xy+\mathrm{i}\,kz\left(x\partial_y+y\partial_x\right)-\left(b^2+z^2\right)\partial_x\partial_y\right] \tag{53}$$

$$L_z=\frac{1}{2\mathrm{i}}\left(\hat{a}_x^\dagger\hat{a}_y-\hat{a}_y^\dagger\hat{a}_x\right)=\frac{\mathrm{i}}{2}\left(y\partial_x-x\partial_y\right) \tag{54}$$

$$L_0=\frac{1}{2}\left(\hat{a}_x^\dagger\hat{a}_x+\hat{a}_y^\dagger\hat{a}_y\right)$$
$$=\frac{1}{4bk}\left[k^2\left(x^2+y^2\right)+2\mathrm{i}\,kz\left(x\partial_x+y\partial_y\right)-2k(b-\mathrm{i}\,z)-\left(b^2+z^2\right)\left(\partial_x^2+\partial_y^2\right)\right]. \tag{55}$$

For fixed mode order N, L_x, L_y, and L_z generate $SU(2)$ transformations within the transverse-mode subspace, analogous to polarization rotations on the Poincaré sphere. For $z=0$ we have [77]

$$L_x u_{\nu\eta}^{HG}(\mathbf{r})=\frac{1}{2}(\nu-\eta)\,u_{\nu\eta}^{HG}(\mathbf{r}), \tag{56}$$

and introducing

$$\hat{a}_\pm^\dagger=\frac{\hat{a}_x^\dagger\pm\mathrm{i}\,\hat{a}_y^\dagger}{\sqrt{2}}, \tag{57}$$

we get

$$u_{\ell p}^{\mathrm{LG}}(\mathbf{r})=\frac{1}{\sqrt{\nu_+!\nu_-!}}\left(\hat{a}_+^\dagger\right)^{\nu_+}\left(\hat{a}_-^\dagger\right)^{\nu_-}u_{00}(\mathbf{r}), \tag{58}$$

$$L_z u_{\ell p}^{LG}(\mathbf{r})=\frac{1}{2}(\nu_+-\nu_-)\,u_{\ell p}^{LG}(\mathbf{r}). \tag{59}$$

where $\ell=\nu_+-\nu_-$, $p=\min(\nu_+,\nu_-)$ and $N=\nu_++\nu_-$.

Let us imagine an experiment, which would change the 'relative phase' δ between $\hat{a}_x^\dagger$ and $\hat{a}_y^\dagger$. This would mean, that $u_{\nu\eta}^{\mathrm{HG}}(\mathbf{r})$ will acquire some additional relative phase equal to $(\nu-\eta)\delta/2$. This can be realized with the mode converter ([74], equations (20)–(22), [78]). In an astigmatic mode converter, this relative phase is produced by the different Gouy-phase shifts accumulated along the two transverse axes. Thus,

$$u_{\ell p}^{\mathrm{LG}}(\mathbf{r})=\frac{1}{\sqrt{\nu_+!\nu_-!}}\frac{\left(\hat{a}_x^\dagger+\mathrm{i}\,\hat{a}_y^\dagger\right)^{\nu_+}}{\sqrt{2}}\frac{\left(\hat{a}_x^\dagger-\mathrm{i}\,\hat{a}_y^\dagger\right)^{\nu_-}}{\sqrt{2}}u_{00}(\mathbf{r}), \tag{60}$$

transforms into

$$u_{\ell p}'^{\mathrm{LG}}(\mathbf{r})=\frac{1}{\sqrt{\nu_+!\nu_-!}}\frac{\left(\mathrm{e}^{\mathrm{i}\,\delta/2}\hat{a}_x^\dagger+\mathrm{i}\,\mathrm{e}^{-\mathrm{i}\,\delta/2}\hat{a}_y^\dagger\right)^{\nu_+}}{\sqrt{2}}\frac{\left(\mathrm{e}^{\mathrm{i}\,\delta/2}\hat{a}_x^\dagger-\mathrm{i}\,\mathrm{e}^{-\mathrm{i}\,\delta/2}\hat{a}_y^\dagger\right)^{\nu_-}}{\sqrt{2}}u_{00}(\mathbf{r}). \tag{61}$$

Let us note, that in each multiplier, $\hat{a}_i^\dagger$ behaves just in the same way as E_i in previous waveplate considerations. Thus, one can depict all the states on the Hermite–Laguerre sphere, which would be a Poincaré-like sphere, constructed for creation operators. One can also consider a fibre bundle associated with such a sphere. Note that it is important, that all the multipliers behave identically. On the one side, just by comparison with a half-waveplate, one may consider the 3-sphere S^3, associated with complex numbers (c_1, c_2), associated with 'state' Φ, which describes the phases of the creation operators:

$$\Phi = c_1\hat{a}_+^\dagger + c_2\hat{a}_-^\dagger \tag{62}$$

$$\Phi_\perp = -c_2^*\hat{a}_+^\dagger + c_1^*\hat{a}_-^\dagger, \tag{63}$$

$$|c_1|^2 + |c_2|^2 = 1. \tag{64}$$

For equation (61), analogously to equation (8), the corresponding coefficients are

$$c_1 = \cos\frac{\delta}{2}, \qquad c_2 = \mathrm{i}\ \sin\frac{\delta}{2}, \tag{65}$$

defined up to an arbitrary common phase factor $\mathrm{e}^{\mathrm{i}\,\alpha}$. The actual state of a beam equation (61) can be written simply as

$$u_{\ell p}^{\prime \mathrm{LG}}(\mathbf{r}) = \frac{1}{\sqrt{\nu_+!\nu_-!}}\Phi^{\nu_+}\Phi_\perp^{\nu_-}u_{00}(\mathbf{r}). \tag{66}$$

For the case of two operators, the geometry is just the same as in the simplest case. However, one should keep in mind that each point on the operator 2-sphere would correspond to some state of the beam (61), which we want to be a point in the total space, so the fibre coordinate corresponds to the phase of the beam. From (66) one can see that, the common phase turns out to be a phase $(\nu_+ - \nu_-)\alpha = l\alpha$, where α corresponds to the 'phase' of the operators Φ. For $\ell \neq 0$, points of a fibre whose phases α differ by $2\pi/|\ell|$ should be considered equivalent, giving rise to a smooth orbifold, namely the lens space $L_{|\ell|,1}$ [79, 80]. This circle bundle has first Chern number ℓ, corresponding to the monopole strength $g = \ell/2$ [81]. The connection form has a similar form, but with multiplier $g = \ell/2$ in (23). Polarization is considered independently, and modified, as before, via the waveplate. If polarization follows the same rotation path, the total phase may be expressed in terms of the TAM projection $m = \ell + \sigma$. Thus, the essential difference from the polarization case lies not in the fibre coordinate itself, which again represents the optical phase, but in the base space and in how its evolution gives rise to the accumulated phase.

For higher-order modes, which consist of, e.g. three basis states, an octant representation of the base space may be useful [82]. In this case, the particular geometry of the whole bundle remains an open question.

4.1. Majorana representation

Let us write again the relations between different indices, and introduce J and μ:

$$J = N/2, \qquad \mu = \ell/2, \tag{67}$$

$$J + \mu = \frac{N+\ell}{2} = \nu_+, \tag{68}$$

$$J - \mu = \frac{N-\ell}{2} = \nu_-, \tag{69}$$

and express the state (58) as follows [83–87]:

$$|J,\mu\rangle = \frac{\left(a_+^\dagger\right)^{J+\mu}}{\sqrt{(J+\mu)!}}\frac{\left(a_-^\dagger\right)^{J-\mu}}{\sqrt{(J-\mu)!}}|0,0\rangle. \tag{70}$$

Let us consider an arbitrary beam of fixed order N:

$$|\Psi\rangle = \sum_{\mu=-J}^{J} c_\mu |J,\mu\rangle = \sum_{\mu=-J}^{J} c_\mu \frac{\left(a_+^\dagger\right)^{J+\mu}\left(a_-^\dagger\right)^{J-\mu}}{\sqrt{(J+\mu)!\,(J-\mu)!}}|0,0\rangle, \tag{71}$$

or, equivalently

$$|\Psi\rangle = \sum_{\mu=-J}^{J} c_\mu \frac{\left(a_+^\dagger\right)^{J+\mu}\left(a_-^\dagger\right)^{-(J+\mu)}}{\sqrt{(J+\mu)!\,(J-\mu)!}}\left(a_-^\dagger\right)^{2J}|0,0\rangle. \tag{72}$$

For $c_J \neq 0$ let $-z_i$ be the roots of the polynomial of a power $2J$ in the variable x (formally one can consider $(a_+^\dagger)(a_-^\dagger)^{-1}$ as x in (72)) and with index shift $J+\mu = i$:

$$\sum_{i=0}^{2J} c_{i-J}\frac{x^i}{\sqrt{(2J-i)!i!}} = 0 \leftrightarrow \frac{c_J}{\sqrt{(2J)!}}\prod_{i=1}^{2J}(x+z_i) = 0. \tag{73}$$

Keeping in mind the fundamental theorem of algebra, one can also write (72) in the same form:

$$|\Psi\rangle = c_J\sqrt{\frac{1}{(2J)!}}\prod_{i=1}^{2J}\left(a_+^\dagger + z_i a_-^\dagger\right)|0,0\rangle. \tag{74}$$

If $c_J = 0$, the polynomial in (73) has degree lower than $2J$. Its finite roots are supplemented by roots at infinity so that their total number remains $2J$. In the factorized state (74), each root at infinity corresponds to a factor $a_-^\dagger$. Thus, we have a correspondence between coefficients c_μ and roots z_i, which can be depicted on the sphere S^2 with the help of stereographic projection. For a Laguerre–Gaussian beam only one c_{μ_0} is non-zero, thus we have $J+\mu_0$ roots $z_i = 0$, and $J-\mu_0$ at infinity. The action of the mode converter rotates the roots collectively.

5. A zoo of Poincaré spheres

There are many different objects called Poincaré spheres in the structured-light literature. Most of them are constructed in the same way: one chooses two orthogonal basis states and considers their linear combinations as in (1). As discussed in section 2 and appendix B, for two states $|N\rangle$ and $|S\rangle$ we can write

$$|\Psi(\theta,\varphi)\rangle = \cos\frac{\theta}{2}|N\rangle + e^{i\varphi}\sin\frac{\theta}{2}|S\rangle, \qquad 0 \leqslant \theta \leqslant \pi, \quad 0 \leqslant \varphi < 2\pi. \tag{75}$$

Thus, in order to define a particular Poincaré-like sphere, one has to specify its two pole states. In the context of structured light and paraxial approximation, we characterize these states by their polarization and topological charge.

One of the first spatial-mode Poincaré spheres was introduced by Padgett and Courtial for first-order modes [15]. In their construction, the two poles correspond to the LG modes with $\ell = +1$ and $\ell = -1$. The same formal construction can be extended to arbitrary ℓ:

$$|N\rangle = |\pi\rangle u^{\mathrm{LG}}_{+\ell,p}, \qquad |S\rangle = |\pi\rangle u^{\mathrm{LG}}_{-\ell,p}, \tag{76}$$

where $|\pi\rangle$ is a fixed polarization state. Thus, polarization does not change on this sphere. This construction is often called the *orbital Poincaré sphere* [88–90].

The term 'orbital' is potentially misleading. In paraxial optics, this index has historically been referred to as an orbital angular momentum. However, ℓ is topological charge and does not define the orbital angular momentum of an individual photon, since the spin and orbital parts of the angular momentum of a massless field are not separable [91, 92]. Thus, *orbital Poincaré sphere* is just a historical name. Moreover, the same name is also used by some authors [28, 76] in a different sense, for a different construction described below.

For $\ell = 1$, the transformation of the state on the sphere equation (76) is produced by the standard astigmatic mode converter [93]. This is not true for higher orders. For example, one can define a sphere with $u^{\mathrm{LG}}_{+2,0}$ and $u^{\mathrm{LG}}_{-2,0}$ at its poles, but the intermediate states on this sphere are not the states produced by a cylindrical-lens converter [17, 18]. The mode converter instead transforms states on the *Hermite–Laguerre sphere* [18] discussed also in section 4. This sphere is constructed for the creation operators $\hat{a}_\pm^\dagger$ introduced in equation (58), while their transformation is given by equation (61). For $N = 1$, the *Hermite–Laguerre sphere* coincides with the *orbital Poincaré sphere* in equation (76). For $N > 1$, powers of the transformed operators produce additional cross terms and, consequently, additional modes of the same order. Therefore, the two constructions may have the same pole modes but different states between the poles.

Higher-order Poincaré spheres are obtained by using both polarization and phase vortex [94]. From equation (39),

$$|N\rangle \sim |R\rangle\, u^{\mathrm{LG}}_{m-1,p}, \qquad |S\rangle \sim |L\rangle\, u^{\mathrm{LG}}_{1-m,p}. \tag{77}$$

The states $|N\rangle$ and $|S\rangle$ have TAM projections $+m$ and $-m$, and topological charges $m-1$ and $1-m$, respectively. This is the higher-order Poincaré sphere considered in section 3. Holleczek *et al* considered two such spaces for first-order cylindrically polarized fields [94] with the difference in the choice of the polar axis.

The *hybrid-order Poincaré sphere* of Yi *et al* is constructed in the same way, but the topological charges of its two poles are independent [95]:

$$|N\rangle \sim |R\rangle\, u^{\mathrm{LG}}_{\ell_1,p}, \qquad |S\rangle \sim |L\rangle\, u^{\mathrm{LG}}_{\ell_2,p} \tag{78}$$

The two polarizations are orthogonal, but ℓ_1 and ℓ_2 do not have to be opposite. For $\ell_2 = -\ell_1$, equation (78) reduces to the higher-order Poincaré sphere above.

The sphere used by Ling *et al* for full Poincaré beams is a particular hybrid-order Poincaré sphere [96]:

$$|N\rangle \sim |R\rangle\, u^{\mathrm{LG}}_{0,0}, \qquad |S\rangle \sim |L\rangle\, u^{\mathrm{LG}}_{\ell,0}. \tag{79}$$

The *generalized Poincaré sphere* of Ren *et al* combines a continuous family of such two-state spheres [97]. For each fixed value of the parameter R_{G}, the corresponding space can be written as

$$|N\rangle \sim |\pi(R_{\mathrm{G}})\rangle\, u^{\mathrm{LG}}_{-\ell,p}, \qquad |S\rangle \sim |\pi^{\perp}(R_{\mathrm{G}})\rangle\, u^{\mathrm{LG}}_{\ell,p}, \qquad \langle \pi^{\perp}(R_{\mathrm{G}}) | \pi(R_{\mathrm{G}})\rangle = 0. \tag{80}$$

The parameter $R_{\mathrm{G}} \in [1/2, 1]$ is represented as the radius of the generalized sphere. A surface with a fixed radius R_{G} is called a spherical shell. Moving from one shell to another changes the ellipticity of the pole polarizations themselves. The radial coordinate labels which orthogonal polarization basis is used to construct the sphere.

Thus, most objects in this 'zoo' differ only in the two states used as their basis. The Hermite–Laguerre sphere is different: it is constructed for creation operators. Finally, for three or more basis states, the full projective state space is no longer a sphere, Poincaré spheres describe only two-state subspaces. Higher-dimensional states require other representations, such as the octant constructions [82].

6. Discussion

We wish to point out that in the literature the term *geometric phase* is not always used consistently. In particular, while for a wave plate the trajectory on the Poincaré sphere is clearly defined and can be parametrized by a real coordinate, this is no longer the case for the corresponding nanoparticle. In a nanoparticle, the polarization cannot be always defined or tracked inside the structure in the same way as in a waveplate, and the associated unitary matrices are therefore introduced in a rather formal sense. Nevertheless, for nanoparticles, the phase can be obtained by a different procedure, namely by rotating the particle and moving to a different reference frame.

For the so-called nonlinear geometric phase, there exists an analogy with this approach [98], however, in this case it is apparently no longer possible, even formally, to introduce a unitary matrix or a closed path [99] on the Poincaré sphere. This raises the question of whether all these phases should indeed be termed geometric, or whether the concept of geometric phase should be extended to a broader class of problems. We regard the strict delineation of this class of phases in optics as an open question for discussion.

We further suggest to reserve the term *Pancharatnam–Berry phase* exclusively for phases whose geometry coincides with that described here and is associated with the Hopf fibration. Other phases, for example, the frequently used illustration (see figure 5) based on parallel transport of a tangent vector on a sphere are indeed geometric phases, but they can be misleading when used in discussions of the Pancharatnam–Berry phase, as they are characterized by a fundamentally different geometry. This picture based on parallel transport of a tangent vector on S^2 corresponds not to the Hopf fibration, but to the unit tangent bundle with a different value of Chern class $c_1(TS^2) = 2$, which is also the Euler class, whereas the Hopf bundle $S^3 \to S^2$ has $c_1 = 1$ [100, 101]. Its total space is $L(2,1) \simeq SO(3) \simeq \mathbb{RP}^3$, rather than S^3. Thus the two constructions define genuinely different circle bundles over the base S^2, even though both have fibre S^1.

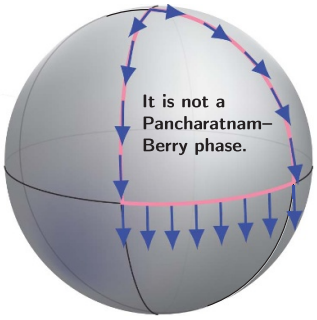


Figure 5. A frequently used illustration of a geometric phase which, however, is not a Pancharatnam–Berry phase and has a different geometry; it is equal to the full solid angle rather than half of it.

Table 1. Summary of the geometrical settings discussed in the tutorial.

Case	Base space	Total space	Phase law	PB?
Polarization waveplate	Poincaré sphere	Hopf bundle	$\Omega/2$, $e^{\pm 2i\beta}$	Yes
Nanostructure, $2m_{\text{out/in}} = n\nu$	Formal Poincaré analogy	Formal Hopf bundle	$\Omega/2$, $e^{i\,(m_{\text{inc}}-m_{\text{out}})\beta}$	Restricted
Arbitrary TAM pair	Formal two-state sphere	Hopf bundle after choosing the two-state subspace	$e^{i\,(m_{\text{inc}}-m_{\text{out}})\beta}$	Weak analogy
HG/LG usual consideration	Hermite–Laguerre sphere	Lens spaces	$\ell\Omega/2$	Not PB
Arrows on sphere, unit tangent bundle	Sphere S^2	$L(2,1) \simeq SO(3) \simeq \mathbb{RP}^3$	Ω	Not PB

Table 1 summarizes the main geometrical settings discussed above. The same rotation-dependent phase factor does not by itself define a unique geometric phase; the relevant distinction is the underlying base space and fibre structure.

Another open issue concerns the non-uniqueness of the connection. The connection discussed here is the canonical one, however, it is in principle possible to introduce other connections that are not related to it by a gauge transformation and that yield different curvature and different holonomy, while still corresponding to the same Chern class. To our knowledge, such situations have not been discussed in the optics literature. Nevertheless, it cannot be excluded that for other physical problems precisely these alternative connections may turn out to be relevant. It might then be expedient to resort to the classical complex algebraic-geometric formalism employed in [102, 103]. On the experimental side, some of the theoretical issues discussed in [104] may be also fruitfully explored.

7. Conclusions

Summing up, in this paper we have analysed the geometric (Pancharatnam) phase, starting from its abstract mathematical definition and establishing an explicit bridge to physical observables through concrete calculations. We have further demonstrated that for vortex beams, an entirely analogous Berry phase can be introduced, which is equal to $\Omega/2$, rather than $\ell\Omega/2$, within a distinct experimental configuration. In the nanostructure setting considered here, rotational symmetry determines which TAM-conversion channels are allowed, while the phase of each channel depends on $m^{\text{inc}} - m^{\text{out}}$. Different spatial modes can therefore respond differently to the same structural rotation. This provides a simple route to mode-selective phase control and discrimination, which may be useful for mode multiplexing in nanophotonic systems. More general multimode and nonlinear cases remain to be explored.

As new types of optical geometric phases continue to emerge, it becomes increasingly important to move beyond heuristic analogies and specify their geometry precisely. Similar phase laws or Poincaré-like representations do not by themselves imply the same underlying mechanism. A formulation in terms of the relevant state space, bundle, and connection provides a common framework in which different geometric phases can be defined, compared, and consistently classified.

Acknowledgments

K F thanks Timur Seidov, Tim Sulimov, Igor Shenderovich, Nikita Belousov, Costantino De Angelis for the fruitful discussions. Part of this work was conducted at the University of Brescia. K F gratefully acknowledges support from the Alexander von Humboldt Foundation.

E M acknowledges the PNRR RESTART project Smart Metasurfaces Advancing Radio Technology (SMART), CUP E63C22002040007, and Erasmus Mundus EMIMEP, CUP D81I24000080006.

M S thanks Gabriele Barbieri for enlightening discussions and collaboration on related topics. His research is supported by UCSC D1-funds and it has been carried out within INDAM-GNSAGA's framework.

The authors acknowledge the use of ChatGPT (OpenAI) for assistance with language editing and improving the clarity of the manuscript.

Data availability statement

No new data were created or analysed in this study.

Author contributions

Kristina Frizyuk 0000-0002-0506-464X
Conceptualization (lead), Formal analysis (lead), Investigation (equal), Methodology (equal), Project administration (equal), Supervision (equal), Validation (supporting), Visualization (equal), Writing – original draft (lead), Writing – review & editing (lead)

Evgenii Menshikov 0009-0003-9168-2421
Formal analysis (supporting), Software (lead), Validation (lead), Visualization (equal), Writing – original draft (equal), Writing – review & editing (equal)

Mauro Spera
Formal analysis (equal), Investigation (equal), Methodology (equal), Project administration (equal), Supervision (equal), Writing – original draft (equal), Writing – review & editing (equal)

Appendix A. Stereographic projection

Let the center of a sphere of radius r be at $(0,0,0)$. Draw a line from the north pole that intersects the sphere and the plane $z=0$ at (x,y,z) and $(X,Y,0)$, respectively (see figure 6). We establish a relationship between the coordinates. From the similarity of triangles,

$$X=\frac{rx}{r-z},\quad Y=\frac{ry}{r-z}. \tag{81}$$

However, we would like to express the sphere coordinates in terms of the plane coordinates. For this, we consider the plane as a complex plane and introduce

$$Z=\frac{r(x+\mathrm{i}\,y)}{r-z},\quad \overline{Z}=\frac{r(x-\mathrm{i}\,y)}{r-z}. \tag{82}$$

Consider

$$Z\overline{Z}=\frac{r^2\left(x^2+y^2\right)}{(r-z)^2}=\frac{r^2\left(r^2-z^2\right)}{(r-z)^2}=\frac{r^2(r+z)}{(r-z)}, \tag{83}$$

from here

$$z=\frac{r\left(Z\overline{Z}-r^2\right)}{\left(Z\overline{Z}+r^2\right)}, \tag{84}$$

$$x=\frac{X(r-z)}{r}=\frac{\left(Z+\overline{Z}\right)(r-z)}{2r}=\frac{r^2\left(Z+\overline{Z}\right)}{\left(Z\overline{Z}+r^2\right)}, \tag{85}$$

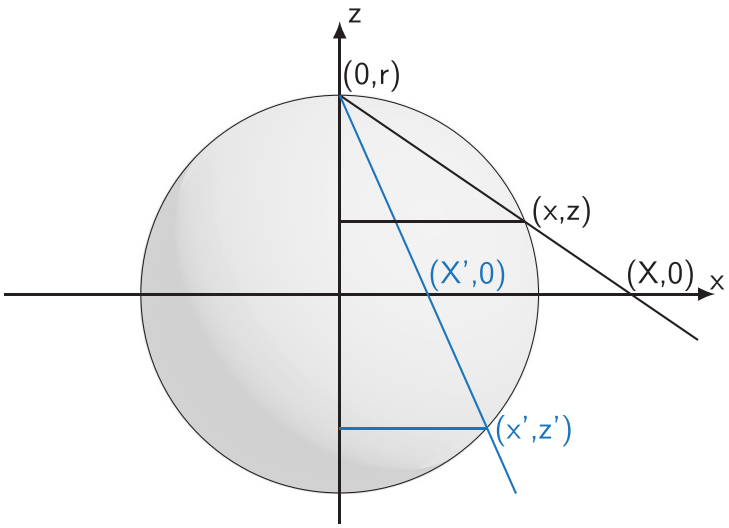


Figure 6. Stereographic projection establishes a one-to-one correspondence between the points on the sphere and those on the plane.

$$y = \frac{Y(r-z)}{r} = \frac{-\mathrm{i}\, r^2 \left(Z-\overline{Z}\right)}{\left(Z\overline{Z}+r^2\right)}. \tag{86}$$

Thus, every point on the sphere, except the north pole, corresponds to a point on the plane. The extended plane includes the point at infinity, which corresponds to the north pole. Stereographic projection preserves angles and generalized circles; that is, it maps circles on the sphere to circles or straight lines on the plane.

Appendix B. Projective space

One can also find a detailed explanation and relation to the Poincaré sphere in [36]. The complex projective space $\mathbb{C}P^n$ is the quotient set $\mathbb{C}^{n+1}\backslash\{0\}$ with respect to the equivalence relation

$$x \sim y \Leftrightarrow \exists \lambda \in \mathbb{C}\backslash\{0\} : x = \lambda y \tag{87}$$

$$\mathbb{C}P^n = \left(\mathbb{C}^{n+1}\backslash\{0\}\right)/\sim \tag{88}$$

One can often encounter notations like $\mathbb{C}\backslash\{0\} := \mathbb{C}^*$. The complex projective line $\mathbb{CP}^1$ is homeomorphic to a sphere, which is also called the Riemann sphere. In other words, the Riemann sphere can be defined as the set of all lines passing through the origin in $\mathbb{C}^2$. Any point on the Riemann sphere can be represented by a pair of complex numbers (z_1, z_2), and two points (z_1, z_2) and (w_1, w_2) represent the same point on the Riemann sphere if there exists a nonzero complex number λ such that:

$$(z_1, z_2) = \lambda\,(w_1, w_2)\,. \tag{89}$$

This equivalence relation introduces the concept of projective coordinates on the Riemann sphere, typically denoted as $[z_1 : z_2]$. The complex plane $\mathbb{C}$ corresponds to the subset of the Riemann sphere where $z_2 \neq 0$, and each point $z \in \mathbb{C}$ is identified with the point $[z_1/z_2 : 1] = [z : 1]$ on the Riemann sphere. The point at infinity is represented by $[1 : 0]$.

Appendix C. Derivations for the $SU(2)$ matrix for the rotated waveplate

The optical axis of the waveplate is rotated by an angle β with respect to the x-axis. We can introduce new $E_{x'}$ and $E_{y'}$ in another coordinate system along the symmetry planes of the waveplate.

In general case it is

$$E_x = \cos\beta E_{x'} - \sin\beta E_{y'}\,, \qquad E_y = \sin\beta E_{x'} + \cos\beta E_{y'} \tag{90}$$

The initial circularly polarized wave is expressed through the new coordinates as

$$E_R = \mathrm{e}^{-\mathrm{i}\beta}\frac{E_{x'} - \mathrm{i}\,E_{y'}}{\sqrt{2}}, \qquad E_L = \mathrm{e}^{\mathrm{i}\beta}\frac{E_{x'} + \mathrm{i}\,E_{y'}}{\sqrt{2}} \tag{91}$$

$$E_{x'} = \frac{\mathrm{e}^{\mathrm{i}\beta}E_R + \mathrm{e}^{-\mathrm{i}\beta}E_L}{\sqrt{2}}, \qquad E_{y'} = -\frac{\mathrm{e}^{\mathrm{i}\beta}E_R - \mathrm{e}^{-\mathrm{i}\beta}E_L}{\mathrm{i}\sqrt{2}} \tag{92}$$

Therefore for electric field components transmitted through a rotated waveplate we have:

$$\tilde{E}_R = \mathrm{e}^{-\mathrm{i}\beta}\left(\mathrm{e}^{\mathrm{i}\,\delta/2}\frac{\mathrm{e}^{\mathrm{i}\beta}E_R + \mathrm{e}^{-\mathrm{i}\beta}E_L}{2} + \mathrm{i}\,\mathrm{e}^{-\mathrm{i}\,\delta/2}\frac{\mathrm{e}^{\mathrm{i}\beta}E_R - \mathrm{e}^{-\mathrm{i}\beta}E_L}{2\mathrm{i}}\right) \tag{93}$$

$$\tilde{E}_L = \mathrm{e}^{\mathrm{i}\beta}\left(\mathrm{e}^{\mathrm{i}\,\delta/2}\frac{\mathrm{e}^{\mathrm{i}\beta}E_R + \mathrm{e}^{-\mathrm{i}\beta}E_L}{2} - \mathrm{i}\,\mathrm{e}^{-\mathrm{i}\,\delta/2}\frac{\mathrm{e}^{\mathrm{i}\beta}E_R - \mathrm{e}^{-\mathrm{i}\beta}E_L}{2\mathrm{i}}\right) \tag{94}$$

$$\tilde{E}_R = \left(\mathrm{e}^{\mathrm{i}\,\delta/2}\frac{E_R + \mathrm{e}^{-2\mathrm{i}\beta}E_L}{2} + \mathrm{e}^{-\mathrm{i}\,\delta/2}\frac{E_R - \mathrm{e}^{-2\mathrm{i}\beta}E_L}{2}\right) \tag{95}$$

$$\tilde{E}_L = \left(\mathrm{e}^{\mathrm{i}\,\delta/2}\frac{\mathrm{e}^{2\mathrm{i}\beta}E_R + E_L}{2} - \mathrm{e}^{-\mathrm{i}\,\delta/2}\frac{\mathrm{e}^{2\mathrm{i}\beta}E_R - E_L}{2}\right) \tag{96}$$

$$\begin{pmatrix}\tilde{E}_R\\ \tilde{E}_L\end{pmatrix} = \begin{pmatrix}\cos\delta/2 & \mathrm{i}\,\mathrm{e}^{-2\mathrm{i}\beta}\sin\delta/2\\ \mathrm{i}\,\mathrm{e}^{2\mathrm{i}\beta}\sin\delta/2 & \cos\delta/2\end{pmatrix}\begin{pmatrix}E_R\\ E_L\end{pmatrix}. \tag{97}$$

So we get the general formula:

$$\begin{pmatrix}\tilde{E}_R\\ \tilde{E}_L\end{pmatrix} = \left(\mathbb{I}\cos\delta/2 + \mathrm{i}\,\left(\cos 2\beta\sigma_x + \sin 2\beta\sigma_y\right)\sin\delta/2\right)\begin{pmatrix}E_R\\ E_L\end{pmatrix}. \tag{98}$$

C.1. Horizontal lift and holonomy: an example

For more general considerations see also the book [51]. Let $\mathcal{A}$ be the global $U(1)$ connection 1–form on S^3. For a lifted curve $z(t) \in S^3 \subset \mathbb{C}^2$ the horizontality is

$$\mathcal{A}\left(\dot{z}(t)\right) = 0. \tag{99}$$

Here we use $z = (z_1, z_2)$ with $z_1 = x_1 + \mathrm{i}\,x_2$, $z_2 = x_3 + \mathrm{i}\,x_4$. Let us fix any (not necessarily horizontal, preferably closed) reference lifted curve $z_{\mathrm{ref}}(t)$ with the same base projection. Any other lift differs by a fibre rotation $\mathrm{e}^{-\mathrm{i}\,\alpha(t)}$, hence

$$z(t) = \mathrm{e}^{-\mathrm{i}\,\alpha(t)}z_{\mathrm{ref}}(t), \qquad \dot{z} = \mathrm{e}^{-\mathrm{i}\,\alpha(t)}\left(\dot{z}_{\mathrm{ref}} - \mathrm{i}\,\dot{\alpha}z_{\mathrm{ref}}\right). \tag{100}$$

Using the $U(1)$–invariance of $\mathcal{A}$ and $\mathcal{A}(u_v) = \mathrm{i}$, the horizontality condition (99) with (100) gives

$$0 = \mathcal{A}\left(\dot{z}\right) = \mathcal{A}\left(\dot{z}_{\mathrm{ref}}\right) - \mathrm{i}\,\dot{\alpha}(t) \quad \Longrightarrow \dot{\alpha}(t) = -\mathrm{i}\,\mathcal{A}\left(\dot{z}_{\mathrm{ref}}(t)\right). \tag{101}$$

In real coordinates on $S^3 \subset \mathbb{R}^4$ we use

$$\begin{aligned}\mathcal{A} &= \mathrm{i}\,\left(x_1\,\mathrm{d}x_2 - x_2\,\mathrm{d}x_1 + x_3\,\mathrm{d}x_4 - x_4\,\mathrm{d}x_3\right),\\ \mathcal{A}\left(\dot{x}\right) &= \mathrm{i}\,\left(x_1\dot{x}_2 - x_2\dot{x}_1 + x_3\dot{x}_4 - x_4\dot{x}_3\right).\end{aligned} \tag{102}$$

Now we consider the example of the closed curve on the Poincaré sphere with a fixed θ and denote $a = \cos(\theta/2)$, $b = \sin(\theta/2)$. A convenient (non-horizontal) closed reference lift of this parallel is given by

$$x_{\mathrm{ref}}(t) = \left(a,\,0,\,b\cos\varphi(t),\,-b\sin\varphi(t)\right), \tag{103}$$

whose Hopf projection is the latitude (parallel) on S^2 with $Z = \cos\theta$. Indeed, $z_1(t) = a$, $z_2(t) = b\cos\varphi(t) - \mathrm{i}\,b\sin\varphi(t) = b\,\mathrm{e}^{-\mathrm{i}\varphi(t)}$, and using the Hopf map (18) we obtain $z_1\overline{z_2} = a\cdot b\,\mathrm{e}^{\mathrm{i}\varphi(t)}$,

$$\pi\left(z_{\mathrm{ref}}(t)\right) = \left(\sin\theta\cos\varphi(t),\,\sin\theta\sin\varphi(t),\,\cos\theta\right).$$

Along this curve the connection form evaluates to

$$\mathcal{A}\left(\dot{x}_{\mathrm{ref}}(t)\right) = -\mathrm{i}\,b^2\,\dot{\varphi}(t) = -\mathrm{i}\,\sin^2\frac{\theta}{2}\,\dot{\varphi}(t) = -\frac{\mathrm{i}}{2}\left(1 - \cos\theta\right)\dot{\varphi}(t). \tag{104}$$

Therefore, the horizontality equation (101) gives

$$\dot{\alpha}(t) = -\mathrm{i}\,\mathcal{A}(\dot{x}_{\mathrm{ref}}(t)) = -\frac{1}{2}(1-\cos\theta)\,\dot{\varphi}(t). \tag{105}$$

For a closed loop along the parallel, φ increases by 2π, hence

$$\begin{aligned}\Delta\alpha &= -\frac{1}{2}\int_0^{2\pi}(1-\cos\theta)\,\mathrm{d}\varphi = -\pi(1-\cos\theta),\\ \mathrm{Hol} &= \exp(-\mathrm{i}\,\Delta\alpha).\end{aligned} \tag{106}$$

Since the solid angle of the spherical cap bounded by the parallel is $\Omega = 2\pi(1-\cos\theta)$, we have the equivalent relation

$$\Delta\alpha \equiv -\frac{1}{2}\Omega, \qquad \mathrm{Hol} = \exp\left(\mathrm{i}\,\frac{\Omega}{2}\right). \tag{107}$$

Note that we could consider a different reference lift, e.g.

$$x_{\mathrm{ref}}(t) = \left(a\cos\frac{\varphi(t)}{2}, a\sin\frac{\varphi(t)}{2}, b\cos\frac{\varphi(t)}{2}, -b\sin\frac{\varphi(t)}{2}\right), \tag{108}$$

and this one is not closed. This means that one should add an additional phase, in this case, π, which corresponds to the non-closedness of the reference lift. This is related to the part of the phase that is referred to as dynamical in [105].

C.2. Global and local descriptions

In practical applications one usually does not work directly with the global connection form $\mathcal{A}$ on the total space E, but rather with its local representatives on the base manifold. This step is often left implicit, but it is important to state it explicitly: obtaining a local connection on the base requires the choice of a local section of the fibre bundle. We introduce angular coordinates on $S^3(\theta,\varphi,\psi)$ with $\theta\in[0,\pi]$, $\varphi\in[0,2\pi)$, and $\psi\in[0,4\pi)$, and write [50]

$$z_1 = \cos\frac{\theta}{2}\exp\left(\mathrm{i}\,\frac{\psi+\varphi}{2}\right), \tag{109}$$

$$z_2 = \sin\frac{\theta}{2}\exp\left(\mathrm{i}\,\frac{\psi-\varphi}{2}\right). \tag{110}$$

The projection $\pi\colon S^3\to S^2$ given by the Hopf map gives

$$x = \sin\theta\cos\varphi, \quad y = \sin\theta\sin\varphi, \quad z = \cos\theta, \tag{111}$$

which is the standard spherical parametrization of S^2. The angles (θ,φ) therefore parametrize the base $B = S^2$, while ψ parametrizes the fibre $F = S^1$.

To pass from the global connection on E to a local gauge potential on B, we need a local section. A (local) section is a smooth map

$$s\colon U\subset B\to E \tag{112}$$

such that $\pi\circ s = \mathrm{id}_U$. For the Hopf bundle we use the canonical sections

$$f_N(\theta,\varphi) = (\theta,\varphi,\psi=-\varphi), \tag{113}$$

$$f_S(\theta,\varphi) = (\theta,\varphi,\psi=+\varphi), \tag{114}$$

defined on the coordinate patches $U_N = S^2\setminus\{\text{south pole}\}$, $U_S = S^2\setminus\{\text{north pole}\}$, respectively, so that each section is smooth on its domain.

Given a connection 1-form $\mathcal{A}$ on E, its local representative on $U\subset B$ is obtained as a pullback along a chosen section s. Let $s\colon B\to E$ be a smooth map and let α be a 1-form on E. The **pullback** of the 1-form α, denoted by $s^*\alpha$, is the 1-form on B defined by

$$(s^*\alpha)_x(v) = \alpha_{s(x)}(s_*v), \tag{115}$$

for any $x \in B$ and $v \in T_xB$, where $s_*: T_xB \to T_{s(x)}E$ is the pushforward. In spherical coordinates the global connection (28) is written as

$$\mathcal{A} = \mathrm{i}\, g(\mathrm{d}\psi + \cos\theta\, \mathrm{d}\varphi). \tag{116}$$

The local connection forms (also called gauge potentials) on U_N and U_S are then defined by

$$A_N := f_N^*\mathcal{A}, \qquad A_S := f_S^*\mathcal{A}.$$

Using (113)–(116) and the fact that f_N and f_S only change ψ, we obtain

$$A_N = f_N^*\mathcal{A} = \mathrm{i}\, g(\mathrm{d}(-\varphi) + \cos\theta\, \mathrm{d}\varphi) = -\mathrm{i}\, g(1-\cos\theta)\, \mathrm{d}\varphi, \tag{117}$$

$$A_S = f_S^*\mathcal{A} = \mathrm{i}\, g(\mathrm{d}\varphi + \cos\theta\, \mathrm{d}\varphi) = \mathrm{i}\, g(1+\cos\theta)\, \mathrm{d}\varphi. \tag{118}$$

These 1-forms A_N and A_S are the local connection forms (gauge potentials) on the base S^2 in the northern and southern charts. On the overlap $U_N \cap U_S$ they are related by the gauge transformation.

C.3. Curvature and Chern classes

A crucial notion is then that of **curvature** of a connection. Given two *horizontal* vector fields u, v, their Lie bracket $([u,v](f) := u\big(v(f)\big) - v\big(u(f)\big))$ is, in general, *not horizontal*: the operator

$$\mathcal{F}(u,v) := -\mathcal{A}([u,v]) \tag{119}$$

is the *curvature* of the given connection. Geometrically, $\mathcal{F}(u,v)$ represents the infinitesimal holonomy associated with a small loop spanned by u and v.

The curvature of a connection is defined globally as the 2-form,

$$\mathcal{F} := \mathrm{d}\mathcal{A} + \mathcal{A}\wedge\mathcal{A}, \tag{120}$$

where $\mathrm{d}\mathcal{A}(u,v) = u\big(\mathcal{A}(v)\big) - v\big(\mathcal{A}(u)\big) - \mathcal{A}\big([u,v]\big)$ for *any* vector fields u, v on E and $(\mathcal{A}\wedge\mathcal{A})(u,v) = [\mathcal{A}(u), \mathcal{A}(v)]$. When dealing with the case of a **principal bundle** — wherein $F = G$, a Lie group, called *structure group* freely acting on fibres, namely, without fixed points — and if G is abelian, the second term will actually *drop out*. So in our case $G = U(1)$ and $\mathcal{F} = \mathrm{d}\mathcal{A}$. Stokes' theorem then yields (pulling back the relevant forms to the base via a local section s so that, slightly abusively, we may look at $\mathcal{F}$ as a 2-form $F := s^*\mathcal{F}$ thereon):

$$\int_{\mathscr{C}} A = \int_{\mathscr{D}} \mathrm{d}A = \int_{\mathscr{D}} F \tag{121}$$

for a loop $\mathscr{C}$ bounding a 2-dimensional domain $\mathscr{D}$ on the base space and where $A = s^*\mathcal{A}$. The holonomy $\mathrm{Hol}_{\mathcal{A}}(\mathscr{C})$ of the connection $\mathcal{A}$ around $\mathscr{C}$, i.e. the (generalized) Berry phase will then be

$$\mathrm{Hol}_{\mathcal{A}}(\mathscr{C}) = \exp\left(-\int_{\mathscr{C}} A\right) = \exp\left(-\int_{\mathscr{D}} F\right). \tag{122}$$

Computing $F = \mathrm{d}A$ from either local potential (117) and (118) gives

$$F_N = \mathrm{d}A_N = -\mathrm{i}\, g\, \mathrm{d}(1-\cos\theta)\wedge\mathrm{d}\varphi = -\mathrm{i}\, g \sin\theta\, \mathrm{d}\theta\wedge\mathrm{d}\varphi, \tag{123}$$

$$F_S = \mathrm{d}A_S = \mathrm{i}\, g\, \mathrm{d}(1+\cos\theta)\wedge\mathrm{d}\varphi = -\mathrm{i}\, g \sin\theta\, \mathrm{d}\theta\wedge\mathrm{d}\varphi. \tag{124}$$

Thus $F_N = F_S =: F$ defines a globally well-defined curvature 2-form on S^2. For a closed curve $\mathcal{C} \subset S^2$ bounding an oriented surface $\mathcal{D}$, Stokes' theorem yields

$$\oint_{\mathcal{C}} A_{N/S} = \iint_{\mathcal{D}} F. \tag{125}$$

Since $\sin\theta\, \mathrm{d}\theta\wedge\mathrm{d}\varphi$ is the area form on the unit sphere, the integral of the curvature over $\mathcal{D}$ equals the solid angle $\Omega(\mathcal{C})$ enclosed by $\mathcal{C}$:

$$\iint_{\mathcal{D}} F = -\mathrm{i}\, g\Omega(\mathcal{C}). \tag{126}$$

Finally, integrating the curvature over the whole sphere gives $\iint_{\mathcal{D}} F = -4\pi \mathrm{i}\, g$. The first Chern number therefore reads

$$c_1 = \frac{1}{-2\pi \mathrm{i}} \iint_{S^2} F = 2g, \tag{127}$$

which reduces to $c_1 = 1$ upon choosing the standard normalization $g = \frac{1}{2}$.

Appendix D. $SU(2)$-actions and parallel transport

We use again $z_1 = x_1 + \mathrm{i}\, x_2$ and $z_2 = x_3 + \mathrm{i}\, x_4$. A vector field is written in the real basis $(\partial_1, \ldots, \partial_4)$. Let $U \in SU(2)$ act on every point of $\mathbb{C}^2(z_1, z_2)$ as follows:

$$\Phi_U : \ (z_1, z_2)^{\mathsf{T}} \mapsto (z_1', z_2')^{\mathsf{T}} = U\,(z_1, z_2)^{\mathsf{T}}. \tag{128}$$

This induces a real linear map $Q \in SO(4)$ (compare with rotation in quaternion form) on $x = (x_1, x_2, x_3, x_4)^{\mathsf{T}}$:

$$x' = Qx. \tag{129}$$

We want to find a vector field on S^3 that corresponds to an infinitesimal rotation generated by such a unitary matrix. Now consider the example $U = \cos\delta/2\ \mathbb{I} + \mathrm{i}\ \sin\delta/2\ \sigma_x$. For this case

$$Q_x = \begin{pmatrix} \cos\delta/2 & 0 & 0 & -\sin\delta/2 \\ 0 & \cos\delta/2 & \sin\delta/2 & 0 \\ 0 & -\sin\delta/2 & \cos\delta/2 & 0 \\ \sin\delta/2 & 0 & 0 & \cos\delta/2 \end{pmatrix}. \tag{130}$$

In the general case (10) we introduce the notation

$$c = \cos\delta/2,\ s = \sin\delta/2, \tag{131}$$

$$c_2 = \cos(2\beta),\ s_2 = \sin(2\beta) \tag{132}$$

and get

$$Q(\delta, \beta) = \begin{pmatrix} c & 0 & ss_2 & -sc_2 \\ 0 & c & sc_2 & ss_2 \\ -ss_2 & -sc_2 & c & 0 \\ sc_2 & -ss_2 & 0 & c \end{pmatrix}, \tag{133}$$

and with an additional σ_z rotation $U = \cos\delta/2\ \mathbb{I} + \mathrm{i}\ \sin\delta/2\ \sigma_z$, which is not realized via the waveplate

$$Q_z = \begin{pmatrix} c & -s & 0 & 0 \\ s & c & 0 & 0 \\ 0 & 0 & c & s \\ 0 & 0 & -s & c \end{pmatrix}. \tag{134}$$

When considering an infinitesimal rotation we should just take the corresponding generator L_Q to get the corresponding vector field as $\dot{x} = L_Q x$, leading to, e.g.

$$L_z = \begin{pmatrix} 0 & -1 & 0 & 0 \\ 1 & 0 & 0 & 0 \\ 0 & 0 & 0 & 1 \\ 0 & 0 & -1 & 0 \end{pmatrix}. \tag{135}$$

With corresponding vector field

$$u_z = -x_2\partial_1 + x_1\partial_2 + \{x_4\partial_3 - x_3\partial_4\}. \tag{136}$$

Analogously,

$$u_x = -x_4\partial_1 + \{x_3\partial_2 - x_2\partial_3\} + x_1\partial_4, \tag{137}$$

$$u_y = \{x_3\partial_1\} + x_4\partial_2 - \{x_1\partial_3\} - x_2\partial_4. \tag{138}$$

Note that they differ from horizontal or vertical vector fields (29) and (30). For convenience, we put the non-matching terms in curly brackets. So, a unitary 1-parameter subgroup realizes a specific motion on S^3 along the vector fields, given above, which are not horizontal. This means that, in general, a point in S^3 does not move in the way prescribed by the connection form (23), and when we have a closed curve on the Poincaré sphere, realized by a $SU(2)$ rotation, the lifted curve on the S^3 sphere is not horizontal (see, for example, figure 3 in [58] as an instance of non-parallel transport). However, for particular lines, where non-coinciding terms for u_x and u_y are zero, we still move along horizontal vector fields! For example, for u_x we want $x_3 = x_2 = 0$, which means that z_1 is purely real and z_2 is purely imaginary. That corresponds to the great circle with $x = 0$ (18). But σ_x corresponds to the rotation of the Poincaré sphere around the x-axis, which means that the motion in S^3 induced by that along a great circle in S^2 is indeed dictated by parallel transport. Similarly, we can consider other rotation angles of the waveplate, however, moving on a great circle of S^2 provides a necessary condition for the phase to be geometric.

Appendix E. Eigenmodes, scattering and irreps

In this section we discuss, how the shape of the nanostructures was chosen based on their scattering properties for a particular vortex beam. As follows from Wigner's theorem [106], if a resonator belongs to a particular symmetry group, i.e., it does not change its shape under all transformations of that group, its eigenmodes transform according to its irreducible representations. This means that eigenmodes of different symmetries can be classified according to the irreducible representations (irreps) [37, 38]. The symmetry behaviour of the scattered wave can also be decomposed into a direct sum of irreps, and a particular mode will be excited only if the same irrep belongs to the decomposition of the incident wave [37, 107].

However, in the case of axially symmetric systems, these considerations may be simplified. We are interested only in a single quantity that describes the symmetry behaviour of the incident wave and the eigenmodes under rotations around the z-axis: the projection of the total angular momentum (TAM). Plane waves and the discussed vortex beams possess a well-defined value of m. But then the nanostructure has $\mathfrak{n}$-fold symmetry. This means that each eigenmode contains all possible values of m that differ by $\mathfrak{n}\nu$, $\nu \in \mathbb{Z}$. Consequently, the function describing this eigenmode may be decomposed into a series, each term of which has the same symmetry behaviour as the exponential $e^{i\,(m_i+\mathfrak{n}\nu)\varphi}$, where m_i is an integer that characterizes the eigenmode. It can be understood with the help of a Fourier-like decomposition of the shape of the nanostructure, written as a function of the angle φ. Rigorous considerations for vector functions can be found in [37], and a simplified scalar version in [107, 108]. Thus, after all, if m is the TAM projection of the incident field, then all eigenmodes for which

$$\exists \nu \in \mathbb{Z}, m = m_i + \mathfrak{n}\nu \tag{139}$$

is valid are excited.

In particular, this means that if we have a triangular nanostructure, $\mathfrak{n} = 3$, and, for example, the incident beam has $m = 3$, then the component with $m = -3$ TAM projection could also contribute to the scattered field, because for the triangular structure, all eigenmodes with TAM projection $3 + 3\nu$ are excited, and for the hexagonal structure, $3 + 6\nu$. However, not only does $m = -3$ contribute to scattering, but also an infinite number of other possible values.

The contribution of each TAM projection depends on the resonances and the particular shape of the structure and can be optimized.

Another way to view this is to keep in mind that two different eigenmodes, or more precisely two different types of eigenmodes, must be excited with different phases. They should be independently excited by

$$|B_e\rangle = \frac{|R\rangle + |L\rangle}{\sqrt{2}} \text{ and } |B_o\rangle = -\mathrm{i}\,\frac{|R\rangle - |L\rangle}{\sqrt{2}}, \tag{140}$$

with different phases and amplitudes. This would be analogous to horizontal and vertical linear polarizations on the Poincaré sphere. This means that such eigenmodes should each transform according to a 1-dimensional irrep, because if they transformed according to a 2-dimensional irrep into each other, they would have the same amplitudes and phases. Group representation theory tells us that this is valid for shapes for which the condition $2m = \mathfrak{n}\nu$ is satisfied, exactly as in the previous case.

E.1. Cases with different TAM projections and another view on the geometry

The higher-order Poincaré sphere is defined based on two basis states, and, in principle, it does not necessarily have to be based on mirror-symmetric states, such as left- and right-polarized plane waves or the previously considered beams. We could also consider a hybrid-order Poincaré sphere and construct something similar for any two arbitrary values of m. Considerations based on irreps are not straightforward in this case and can be misleading, because now the modes can transform according to any irrep. However, the selection rules, which determine whether a mode with another m will be excited, are still valid:

$$m^{\mathrm{inc}} - m^{\mathrm{out}} = \mathfrak{n}\nu. \tag{141}$$

But how can we now determine, which phase is obtained during rotation of the nanostructure? We can, in principle, follow the same approach as described in [69, 98, 109]. For this, we consider a system consisting of a nanostructure irradiated by a particular TAM component and a particular TAM component of the scattered field, and first rotate the system as a whole by an angle β. The incident and scattered fields acquire the phases $\mathrm{e}^{-\mathrm{i}\ m^{\mathrm{out/inc}}\beta}$, each with its own value of m. Then, we perform a time shift such that the incident field coincides with the one before rotation. This corresponds to the same incident field, but a rotated nanostructure. The scattered field already has the phase $\mathrm{e}^{-\mathrm{i}\ m^{\mathrm{out}}\beta}$, and after the time shift it acquires an additional phase $\mathrm{e}^{\mathrm{i}\ m^{\mathrm{inc}}\beta}$, because it has the same frequency as the incident field. This gives the expression (43). Note that here we did not use the language of unitary matrices at all, nor did we consider any real path on the Poincaré sphere and its holonomy.

The geometric interpretation of this phase remains quite formal and may be somewhat forced. It again raises the question of the definition of the geometric phase in physics: should the holonomy interpretation be necessary, or can one just rely on the vague idea that 'the phase depends somehow only on the geometry, but not on the resonances', which, of course, does not yet constitute a rigorous definition but may possibly be refined.

Appendix F. Interpretation in terms of coherent states

The preceding observations could be rephrased via Perelomov's coherent states ([87, 110, 111], see also [104]). In physical terms, let us choose a state on the Poincaré sphere, for instance, a pole. Any transformation that belongs to the group $SU(2)$ can either move the state to another one, which corresponds to a different point on the sphere, or just introduce some phase (for the pole it would be the subgroup of rotations around the z-axis). In mathematical terms, we consider an action of a compact Lie group G ($SU(2)$ in our case) on a finite-dimensional vector space V (space of polarization states) and obtain the orbit of this action on a vector $|\xi\rangle \in V$:

$$\mathcal{O}_\xi = \{[U(g)\,|\xi\rangle]\ |\, g \in G\} \cong G/H. \tag{142}$$

where H, called the isotropy group of $|\xi\rangle$ (in our case H is $U(1)$ and G/H is topologically S^2), satisfies

$$U(h)\,|\xi\rangle = \mathrm{e}^{\mathrm{i}\ \{\alpha(h)\}}|\xi\rangle \tag{143}$$

with $\mathrm{e}^{\mathrm{i}\ \alpha(\cdot)}$ a character of H, namely, a one-dimensional representation of H:

$$\mathrm{e}^{\mathrm{i}\ \{\alpha(h_1h_2)\}} = \mathrm{e}^{\mathrm{i}\ \{\alpha(h_1)\}}\,\mathrm{e}^{\mathrm{i}\ \{\alpha(h_2)\}}, \quad h_1, h_2 \in H. \tag{144}$$

The above arrangement is termed a *coherent state system associated with the representation* $U(\cdot)$ *and the vector* $|\xi\rangle$. Physically, coherent states are all possible states which can be obtained from a given one by an action of the group. Ultimately, we have a principal bundle with structure group H and base manifold G/H.

A unitary irreducible representation $U(\cdot)$ of $G = SU(2) \cong S^3$ is labelled by its 'spin' J and it has dimension $2J+1$. For the Poincaré-sphere orbit considered here, $H = U(1) \cong SO(2) \approx S^1$. Upon taking the corresponding reference vector $|\xi\rangle \in V_J$ and acting thereon via the representation, we obtain the coherent-state manifold

$$\{[U(g)\,|\xi\rangle]\ |\, g \in SU(2)\} \cong SU(2)/U(1) \cong S^2. \tag{145}$$

Appendix G. Details of numerical simulations

We numerically calculate the phase ϕ of the electric field acquired by rotation of a silicon particle exhibiting different symmetries under illumination by a circularly polarized paraxial Laguerre–Gaussian beam

$$\mathbf{E}_{\text{inc}} \propto (\hat{\mathbf{x}} \pm \mathrm{i}\, \hat{\mathbf{y}})\, u_{lp}^{\text{LG}}(\mathbf{r}). \tag{146}$$

TAM projection m of such an input field can be obtained by writing the expression for a circularly polarized field in equivalent form (see equations (39), (47) and (48))

$$\mathbf{E}_{lp}^{\pm} = \mathrm{e}^{\pm \mathrm{i}\varphi}\, (\hat{\boldsymbol{\rho}} \pm \mathrm{i}\, \hat{\boldsymbol{\varphi}})\, u_{lp}^{LG}(\mathbf{r}). \tag{147}$$

Combining the angular dependencies $\mathrm{e}^{\pm \mathrm{i}\varphi}\mathrm{e}^{\mathrm{i}\, l\varphi}$, for the TAM projection of an LG beam we have $m = l \pm 1$. The phase acquired by the rotation of the particle under excitation with a beam ($\lambda = 1550$ nm) having TAM-projection m was determined as follows:

$$\phi_{\pm m} = \arg\left[\int_S \mathbf{E}(\rho, \varphi, z_0) \cdot (\hat{\boldsymbol{\rho}} \mp \mathrm{i}\, \hat{\boldsymbol{\varphi}})\, \mathrm{e}^{\mp \mathrm{i}\, m\varphi} \mathrm{d}S\right], \tag{148}$$

where the upper(lower) sign corresponds to the right(left) hand light helicity; the integration was performed over the surface positioned below the particle ($z_0 = -1$ μm). Geometrical parameters of the particles were the following: D_{2h} particle width $w = 263$ nm, height $h = 790$ nm, depth $d = 345$ nm; D_{6h} particle $w = 291$ nm, $h = 700$ nm, the radius of the inscribed circle $R = 922$ nm; D_{3h} particle $w = 591$ nm, $h = 700$ nm, $R = 1300$ nm. Calculations were performed using COMSOL Multiphysics™ software.

Appendix H. Horizontal lift and the usual Berry integral

In this section, we provide a correspondence between the standard notation, e.g. in [4, 29, 112], and the present approach. Let $z = (z_1, z_2) \in S^3 \subset \mathbb{C}^2$ be a normalized representative of a polarization state. We use the Hermitian product (20): $\langle z|w\rangle = \overline{z_1} w_1 + \overline{z_2} w_2$. Let $z \in S^3 \subset \mathbb{C}^2$ be a normalized representative of a *ray* (ray $[z] \in \mathbb{C}P^1$ is the physical state defined up to an overall phase [113–115]),

$$\langle z|z\rangle = 1. \tag{149}$$

Consider another normalized representative z' of a neighbouring ray. The Pancharatnam condition says that the two states are in phase if [3, 114]

$$\langle z|z'\rangle \in \mathbb{R}_+. \tag{150}$$

Now let the neighbouring representative be obtained from a smooth curve $z(t) \in S^3$,

$$z' = z(t + \mathrm{d}t) = z(t) + \dot{z}(t)\, \mathrm{d}t. \tag{151}$$

Then

$$\langle z(t)\, |z(t + \mathrm{d}t)\rangle = 1 + \langle z(t)\, |\dot{z}(t)\rangle\, \mathrm{d}t. \tag{152}$$

Since the curve stays on S^3, we have

$$\frac{\mathrm{d}}{\mathrm{d}t}\langle z(t)\, |z(t)\rangle = 0, \text{ therefore, } \langle \dot{z}(t)\, |z(t)\rangle + \langle z(t)\, |\dot{z}(t)\rangle = 0, \tag{153}$$

and hence

$$\mathrm{Re}\langle z(t)\, |\dot{z}(t)\rangle = 0. \tag{154}$$

Thus $\langle z(t)|\dot{z}(t)\rangle$ is purely imaginary. The Pancharatnam condition requires

$$\langle z(t)\, |z(t + \mathrm{d}t)\rangle \in \mathbb{R}_+. \tag{155}$$

Using the previous expressions, we get both $\mathrm{Im}\langle z(t)|\dot{z}(t)\rangle = 0$ and $\mathrm{Re}\langle z(t)|\dot{z}(t)\rangle = 0$, which means

$$\langle z(t)\,|\dot{z}(t)\rangle = 0. \tag{156}$$

This is precisely the condition that the tangent vector $\dot{z}(t)$ belongs to the horizontal space defined in equation (22), and can be also found in, e.g. [26]. Therefore, the horizontal space consists of those infinitesimal changes of the representative which keep neighbouring states in phase in the Pancharatnam sense.

Note, that (compare with (99))

$$\mathcal{A}(\dot{z}) = \mathrm{i}\ (x_1\dot{x}_2 - x_2\dot{x}_1 + x_3\dot{x}_4 - x_4\dot{x}_3) = \mathrm{i}\ \mathrm{Im}\langle z|\dot{z}\rangle = \langle z|\dot{z}\rangle. \tag{157}$$

The same object is usually written in Berry's notation after choosing a local reference lift. Let the base point be denoted by $\mathbf{R}$, and let $z_{\mathrm{ref}}(\mathbf{R})$ be a chosen normalized representative of the corresponding ray. For a curve $\mathbf{R}(t)$ on the base, the reference lift is

$$z_{\mathrm{ref}}(t) = z_{\mathrm{ref}}(\mathbf{R}(t)), \qquad \langle z_{\mathrm{ref}}(t)|\dot{z}_{\mathrm{ref}}(t)\rangle = \langle z_{\mathrm{ref}}(\mathbf{R})|\nabla_{\mathbf{R}} z_{\mathrm{ref}}(\mathbf{R})\rangle \cdot \dot{\mathbf{R}}. \tag{158}$$

Therefore, in this local gauge, the usual Berry phase along a closed curve C is

$$\gamma_{\mathrm{B}}[C] = \mathrm{i} \oint_C \langle z_{\mathrm{ref}}(\mathbf{R})|\nabla_{\mathbf{R}} z_{\mathrm{ref}}(\mathbf{R})\rangle \cdot \mathrm{d}\mathbf{R}. \tag{159}$$

Equivalently,

$$\gamma = \mathrm{i} \oint_C \langle z_{\mathrm{ref}}|\,\mathrm{d}z_{\mathrm{ref}}\rangle. \tag{160}$$

This is the same connection as above.

References

[1] Cisowski C, Götte J B and Franke-Arnold S 2022 *Rev. Mod. Phys.* **94** 031001
[2] Cohen E, Larocque H, Bouchard F, Nejadsattari F, Gefen Y and Karimi E 2019 *Nat. Rev. Phys.* **1** 437–49
[3] Pancharatnam S 1956 *Proc. Indian Acad. Sci.* **44** 247–62
[4] Berry M 1987 *J. Mod. Opt.* **34** 1401–7
[5] Ding X, Monticone F, Zhang K, Zhang L, Gao D, Burokur S N, de Lustrac A, Wu Q, Qiu C W and Alù A 2015 *Adv. Mater.* **27** 1195–200
[6] Luo W, Sun S, Xu H X, He Q and Zhou L 2017 *Phys. Rev. Appl.* **7** 044033
[7] Huang L, Chen X, Mühlenbernd H, Li G, Bai B, Tan Q, Jin G, Zentgraf T and Zhang S 2012 *Nano Lett.* **12** 5750–5
[8] Khorasaninejad M, Chen W T, Devlin R C, Oh J, Zhu A Y and Capasso F 2016 *Science* **352** 1190–4
[9] Wen D *et al* 2015 *Nat. Commun.* **6** 8241
[10] Zheng G, Mühlenbernd H, Kenney M, Li G, Zentgraf T and Zhang S 2015 *Nat. Nanotechnol.* **10** 308–12
[11] Marrucci L, Manzo C and Paparo D 2006 *Appl. Phys. Lett.* **88** 221102
[12] Xie X, Pu M, Jin J, Xu M, Guo Y, Li X, Gao P, Ma X and Luo X 2021 *Phys. Rev. Lett.* **126** 183902
[13] Deng Q, Yang J, Lan X, Zhang W, Cui H, Xie Z, Li L and Huang Y 2023 *Results Phys.* **51** 106730
[14] Galvez E J, Crawford P R, Sztul H I, Pysher M J, Haglin P J and Williams R E 2003 *Phys. Rev. Lett.* **90** 203901
[15] Padgett M J and Courtial J 1999 *Opt. Lett.* **24** 430–2
[16] van Enk S J 1993 *Opt. Commun.* **102** 59–64
[17] Habraken S J M and Nienhuis G 2010 *Opt. Lett.* **35** 3535–7
[18] Habraken S J M and Nienhuis G 2010 Geometric phases in higher-order transverse optical modes *Proc. Complex Light and Optical Forces IV* vol 7613 (SPIE) pp 121–8
[19] Tomita A and Chiao R Y 1986 *Phys. Rev. Lett.* **57** 937–40
[20] Bliokh K Y, Niv A, Kleiner V and Hasman E 2008 *Nat. Photon.* **2** 748–53
[21] Zhen W, Wang X L, Ding J and Wang H T 2023 *Phys. Rev. A* **108** 023514
[22] Zhen W, Ren Z C, Wang X L, Ding J and Wang H T 2025 *Sci. China Phys. Mech. Astron.* **68** 244211
[23] Wang J *et al* 2023 *Nat. Photon.* **17** 120–5
[24] Palmerduca E and Qin H 2024 *Phys. Rev. D* **109** 085005
[25] Cao Z X, Liu T T, Zhao B, Rosales-Guzmán C, Liu J and Zhu Z H 2024 *Opt. Express* **32** 28025–34
[26] Simon B 1983 *Phys. Rev. Lett.* **51** 2167–70
[27] Cayssol J and Fuchs J N 2021 *J. Phys.: Mater.* **4** 034007
[28] Rao A S 2026 *Adv. Photonics Res.* **7** e70220
[29] Jisha C P, Nolte S and Alberucci A 2021 *Laser Photonics Rev.* **15** 2100003
[30] Guo Y, Pu M, Zhang F, Xu M, Li X, Ma X and Luo X 2022 *Photonics Insights* **1** R03
[31] Hu Z and Li G 2025 *Appl. Phys. Lett.* **126** 100502
[32] Berry M V 1984 *Proc. R. Soc. A* **392** 45–57
[33] Takenaka H 1973 *Nouv. Rev. Opt.* **4** 37
[34] Sugic D, Droop R, Otte E, Ehrmanntraut D, Nori F, Ruostekoski J, Denz C and Dennis M R 2021 *Nat. Commun.* **12** 1–10

[35] Jurčo B 1987 *Czech. J. Phys.* **37** 1035–8
[36] Vektorfeld 2025 From Poincaré sphere (Bloch sphere) to Projective space (available at: www.youtube.com/watch?v=Qun3gahLP3o)
[37] Gladyshev S, Frizyuk K and Bogdanov A 2020 *Phys. Rev. B* **102** 075103
[38] Xiong Z, Yang Q, Chen W, Wang Z, Xu J, Liu W and Chen Y 2020 *Opt. Express* **28** 3073–85
[39] Shumitskaya A A, Kozlov V O, Selivanov N I, Stoumpos C C, Zapasskii V S, Kapitonov Y V and Ryzhov I I 2024 *Adv. Opt. Mater.* **12** 2302095
[40] Garrison J C and Chiao R Y 1988 *Phys. Rev. Lett.* **60** 165–8
[41] Zee A 2016 *Group Theory in a Nutshell for Physicists* (Princeton University Press)
[42] Saito S 2023 *Front. Phys.* **11** 1225419
[43] Saito S 2024 *Front. Phys.* **11** 1225334
[44] Mechanic Q 2021 Physics Stack Exchange (available at: https://physics.stackexchange.com/q/638919)
[45] del Castillo G F T and Rubalcava-Garcia I 2013 (arXiv:1303.4496)
[46] Yu L, Singh H J, Pietila J and Caglayan H 2026 *Light Sci. Appl.* **15** 119
[47] Liu C, Bai Y, Zhao Q, Yang Y, Chen H, Zhou J and Qiao L 2016 *Sci. Rep.* **6** 34819
[48] Lalanne P and Chavel P 2017 *Laser Photonics Rev.* **11** 1600295
[49] Schuller F P 2015 Institute for Quantum Gravity, Friedrich-Alexander Universität Erlangen-Nürnberg
[50] Chruściński D and Jamiołkowski A 2004 *Geometric Phases in Classical and Quantum Mechanics* (Birkhäuser) (available at: https://link.springer.com/book/10.1007/978-0-8176-8176-0)
[51] Nakahara M 2003 *Geometry, Topology and Physics* (*Graduate Student Series in Physics*) 2nd edn (CRC Press)
[52] Anandan J and Stodolsky L 1987 *Phys. Rev. D* **35** 2597–600
[53] Anandan J 1992 *Nature* **360** 307–13
[54] Johnson N 2011 Hopf fibration – fibers and base (available at: www.youtube.com/watch?v=AKotMPGFJYk)
[55] Urbantke H 1991 *Am. J. Phys.* **59** 503–9
[56] Voitiv A A, Lusk M T and Siemens M E 2023 *Opt. Lett.* **48** 2680–3
[57] Hagen N and Garza-Soto L 2024 *J. Opt. Soc. Am. A* **41** 2014–22
[58] Courtial J 1999 *Opt. Commun.* **171** 179–83
[59] Shen Y 2021 *J. Opt.* **23** 124004
[60] Tung W K 2020 Group Theory In Physics: An Introduction To Symmetry Principles, Group Representations *And Special Functions In Classical And Quantum Physics* (World Scientific) (available at: www.amazon.com/Group-Theory-Physics-Introduction-Representations/dp/0000989754@)
[61] Menshikov E, Franceschini P, Frizyuk K, Fernandez-Corbaton I, Tognazzi A, Cino A C, Garoli D, Petrov M, de Ceglia D and De Angelis C 2025 *Light Sci. Appl.* **14** 381
[62] Nikitina A and Frizyuk K 2024 *Adv. Opt. Mater.* **12** 2400732
[63] Zhan Q 2006 *Opt. Lett.* **31** 867–9
[64] Song Q *et al* 2020 *Nat. Commun.* **11** 1–8
[65] Overvig A C, Shrestha S, Malek S C, Lu M, Stein A, Zheng C and Yu N 2019 *Light Sci. Appl.* **8** 1–12
[66] Hasman E, Kleiner V, Biener G and Niv A 2003 *Appl. Phys. Lett.* **82** 328–30
[67] Larocque H, Gagnon-Bischoff J, Bouchard F, Fickler R, Upham J, Boyd R W and Karimi E 2016 *J. Opt.* **18** 124002
[68] Suzuki M, Yamane K, Oka K, Toda Y and Morita R 2016 *Phys. Rev.* A **94** 043851
[69] Guercio G, Gerini A, Frizyuk K, Morassi M, Lemaitre A, De Angelis C, Carletti L and Leo G 2026 *ACS Photonics* **13** 3134–40
[70] Lax M, Louisell W H and McKnight W B 1975 *Phys. Rev. A* **11** 1365–70
[71] Nienhuis G and Allen L 1993 *Phys. Rev. A* **48** 656–65
[72] Kogelnik H and Li T 1966 *Appl. Opt.* **5** 1550–67
[73] Nienhuis G and Visser J 2004 *J. Opt. A: Pure Appl. Opt.* **6** S248
[74] Beijersbergen M W, Allen L, van der Veen H E L O and Woerdman J P 1993 *Opt. Commun.* **96** 123–32
[75] Dennis M R and Alonso M A 2017 *Philos. Trans. R. Soc. A* **375** 20150441
[76] Calvo G F 2005 *Opt. Lett.* **30** 1207–9
[77] Simon R and Agarwal G S 2000 *Opt. Lett.* **25** 1313–5
[78] Allen L, Courtial J and Padgett M J 1999 *Phys. Rev. E* **60** 7497–503
[79] Albers P, Geiges H and Zehmisch K 2023 *Arnold Math. J.* **9** 41–68
[80] Randy S 2024 The Hopf Fibration: an Example of a Nontrivial Principal Bundle (available at: www.cphysics.org/article/03838.pdf)
[81] Bruzzo U, Fré P, Shahzad U and Trigiante M 2023 *Lett. Math. Phys.* **113** 64–70
[82] Cisowski C 2026 *Phys. Rev. A* **113** 063530
[83] Lee C H and Tan C H 2022 *Topology and Geometry of 3-Band Models IRC-SET 2021* (Springer) pp 59–81
[84] Schwinger J 2015 *On Angular Momentum (Dover Books on Physics)* (Dover Publications) (available at: www.amazon.com/Angular-Momentum-Dover-Books-Physics/dp/0486788105)
[85] Shabbir S 2017 Majorana Representation in Quantum Optics : SU(2) Interferometry and Uncertainty Relations *PhD Thesis* KTH Royal Institute of Technology (available at: www.diva-portal.org/smash/record.jsf?pid=diva2)
[86] Majorana E 1932 *Nuovo Cim.* **9** 43–50
[87] Gutiérrez-Cuevas R, Wadood S A, Vamivakas A N and Alonso M A 2020 *Phys. Rev. Lett.* **125** 123903
[88] Chithrabhanu P, Reddy S G, Anwar A and Singh R P 2015 Generalized orbital angular momentum Poincaré sphere *Int. Conf. on Optics and Photonics 2015* vol 9654 (SPIE) p 409
[89] Karimi E, Slussarenko S, Piccirillo B, Marrucci L and Santamato E 2010 *Phys. Rev. A* **81** 053813
[90] Yang J, Jiang J, Wang J and Zheng X 2025 *Adv. Phys. Res.* **4** 2400083
[91] Palmerduca E and Qin H 2025 *SciPost Phys.* **18** 188
[92] Fernandez-Corbaton I, Zambrana-Puyalto X and Molina-Terriza G 2012 *Phys. Rev. A* **86** 042103
[93] Lassen M, Leuchs G and Andersen U L 2009 *Phys. Rev. Lett.* **102** 163602
[94] Holleczek A, Aiello A, Gabriel C, Marquardt C and Leuchs G 2011 *Opt. Express* **19** 9714–36
[95] Yi X, Liu Y, Ling X, Zhou X, Ke Y, Luo H, Wen S and Fan D 2015 *Phys. Rev. A* **91** 023801
[96] Ling X, Yi X, Dai Z, Wang Y and Chen L 2016 *J. Opt. Soc. Am. B* **33** 2172–6
[97] Ren Z C, Kong L J, Li S M, Qian S X, Li Y, Tu C and Wang H T 2015 *Opt. Express* **23** 26586–95

[98] Tymchenko M, Gomez-Diaz J S, Lee J, Nookala N, Belkin M A and Alù A 2015 *Phys. Rev. Lett.* **115** 207403
[99] Suzuki M, Yamane K, Oka K, Toda Y and Morita R 2016 Comment on "Higher order Pancharatnam-Berry phase and the angular momentum of light" (arXiv:1602.02471)
[100] Hatcher A 2017 Vector bundles and k-theory available from the author's webpage
[101] Davis J F and Kirk P 2001 *Lecture Notes in Algebraic Topology* (American Mathematical Society)
[102] Sansonetto N and Spera M 2010 *J. Geom. Phys.* **60** 501–12
[103] Penna V and Spera M 1998 *J. Geom. Phys.* **27** 99–112
[104] Barbieri G, Frizyuk K and Spera M 2025 Available at SSRN 5371800
[105] Bliokh K Y, Alonso M A and Dennis M R 2019 *Rep. Prog. Phys.* **82** 122401
[106] Sólyom J and Piróth A 2007 *Fundamentals of the Physics of Solids* (Springer)
[107] Tsimokha M, Igoshin V, Nikitina A, Toftul I, Frizyuk K and Petrov M 2022 *Phys. Rev. B* **105** 165311
[108] Vektorfeld 2026 Selection rules for scattering by nanostructures |Optics| Acoustics (available at: www.youtube.com/watch?v=YZ1U6y6Fq10)
[109] Li G, Chen S, Pholchai N, Reineke B, Wong P W H, Pun E Y B, Cheah K W, Zentgraf T and Zhang S 2015 *Nat. Mater.* **14** 607–12
[110] Perelomov A 1986 *Generalized Coherent States and Their Applications* (Springer) (available at: https://link.springer.com/book/10.1007/978-3-642-61629-7)
[111] Kuratsuji H 2013 *Phys. Rev. A* **88** 033801
[112] Born M and Fock V 1928 *Z. Phys.* **51** 165–80
[113] Lévay P 2005 (arXiv:math-ph/0509064)
[114] De Zela F 2012 The Pancharatnam-Berry phase: theoretical and experimental aspects *Theoretical Concepts of Quantum Mechanics* (IntechOpen) (https://doi.org/10.5772/34882)
[115] Weinberg S 1995 *The Quantum Theory of Fields, Volume 1: Foundations* (Cambridge University Press) (https://doi.org/10.1017/CBO9781139644167)